A NEUROVASCULAR COUPLING MODEL BASED ON NITRIC OXIDE AND CARBON DIOXIDE AND ITS VALIDATION WITH TWO-PHOTON MICROSCOPY IMAGING

by

Meryem Ayşe Yücel

BSc, Chemical Engineering, Boğaziçi University, 2003

MSc, Biomedical Engineering, Boğaziçi University, 2005

Submitted to the Institute of Biomedical Engineering

in partial fulfillment of the requirements

for the degree of

Doctor

of

Philosophy

Boğaziçi University

January 2010

A NEUROVASCULAR COUPLING MODEL BASED ON NITRIC OXIDE AND CARBON DIOXIDE AND ITS VALIDATION WITH TWO-PHOTON MICROSCOPY IMAGING

APPROVED BY:

Assoc. Prof. Ata Akın .....
(Thesis Advisor)

Prof. Tamer Demiralp .....

Prof. Ahmet Ademoğlu .....

Prof. Kutlu Ülgen .....

Prof. Hale Saybaşılı .....

DATE OF APPROVAL: 14.Jan.2010

ACKNOWLEDGMENTS

Thanks be to the One to whom belongs all praise.

I would like to express my deep and sincere gratitude to my supervisor, Professor Ata Akın. His wide knowledge, understanding, encouraging, guidance and support throughout this work have provided a good basis for this thesis.

I am deeply grateful to Professor David Boas from Harvard-MIT with whom I have been very privileged to work with on theory, and also to perform the experimental part of this work. I appreciate his advice, comments, and willingness to discuss any questions or ideas I had, and for providing an excellent and inspiring working atmosphere. It was a pleasure for me to work with all the wonderful people at Martinos Center. Among them, I would particularly like to express my deep gratitude to Vivek Srinivasan and Sava Sakadzic for helping me run all the experiments, for their invaluable assistance, as well as for their warm friendship. I would also like to thank Svetlana Ruvinskaya and Weicheng Wu for their technical support during the experiments. I am also grateful to Professor Anna Devor and Qianqian Fang for their insightful discussions.

I also wish to thank to my thesis committee members: Professor Tamer Demiralp, Professor Ahmet Ademoğlu, Professor Kutlu Ülgen and Professor Hale Saybaşılı, and journal paper referees: Professor Kamil Uludağ from Max-Planck Institute and Professor Fahmeed Hyder from Yale University for their constructive criticism and advice during the preparation of this work. I owe a sincere gratitude to Professor Robert Costalat from University of Pierre et Marie Curie for his valuable advice and friendly help throughout this work.

My thanks would not be complete without acknowledging all my friends at Boğaziçi University and at Harvard University who made this period an enjoyable

time for me.

Among last but not least, I owe my loving thanks to my mom, my dad, my sister, my brother and my little İlya for their unflagging love and support throughout my whole life. Without their encouragement and understanding it would have been impossible for me to finish this work.

The financial support of the TÜBİTAK BİDEB and NIH are also gratefully acknowledged.

ABSTRACT

A NEUROVASCULAR COUPLING MODEL BASED ON NITRIC OXIDE AND CARBON DIOXIDE AND ITS VALIDATION WITH TWO-PHOTON MICROSCOPY IMAGING

Understanding neurovascular coupling is of paramount importance since while a normal coupling is vital for a healthy functioning brain, the impairment in coupling is the underlying factor of many neurodegenerative diseases. With this motivation, we aimed to test the still-debatable hypotheses and important aspects of neurovascular coupling: whether the coupling is controlled metabolically or neurogenically, how the coupling is propagated, what kinetics the cerebral metabolic rate of oxygen ($CMRO_2$) follows during neuronal activity and the transient characteristics of the response during stimulus and after stimulus periods. We have modified recent models of neurovascular coupling adding the effects of both nitric oxide (NO) kinetics, a well-known neurogenic vasodilator, and CO_2 kinetics as a metabolic vasodilator to test the neurogenic and metabolic hypotheses. Using 2-photon microscopy imaging, we measured the vessel diameter changes *in vivo* in somatosensory cortex of Sprague Dawley rats during forepaw stimulation to investigate response transients and to test retrograde dilation hypothesis. Our results show that the dominant factor in the hemodynamic response is NO, however CO_2 is important in modulating the shape of the response: causing post-stimulus undershoot due to the washout effect of cerebral blood flow (CBF) resulting in hypocapnia. The statistical analysis of our experimental results and their comparison with the modeling results give more insight into the transient characteristics of the response. Our results support retrograde dilation hypothesis and suggests a $CMRO_2$ onset and return kinetics in seconds rather than in minutes during functional activity.

Keywords: Neurovascular coupling, Neurogenic hypothesis, Metabolic hypothesis, Nitric oxide, Carbon dioxide, 2-photon microscopy.

ÖZET

NİTRİK OKSİT VE KARBON DİOKSİT ÜZERİNE KURULMUŞ SİNİR-DAMAR ETKİLEŞİMİ MODELİ VE MODELİN 2-IŞIN MİKROSKOBU YARDIMIYLA DOĞRULANMASI

Sinir-damar etkileşimini anlamak çok önemlidir, çünkü sinir-damar etkileşimi hem normal beyin işlevleri için hayati öneme sahiptir hem de etkileşimdeki bozukluk bir çok nörodejeneratif hastalığın altyapısını oluşturmaktadır. Buradan yola çıkarak, sinir-damar etkileşimi hakkında hala tartışılan: etkileşimin metabolik yolla mı nörojenik yolla mi kontrol edildiği, oluştuktan sonra ne yönde ilerlediği, uyarı esnasındaki ve uyarı sonrasındaki hemodinamik tepkinin zamansal karakteristiği ve sinir aktivitesi esnasında artan oksijen kullanımının kinetiği hakkındaki en önemli hipotezlere bir cevap vermeyi amaçladık. Nörojenik ve metabolik hipotezleri incelemek için literatürde var olan modellere nörojenik bir damar genişletici olan nitrik oksidin (NO) ve metabolik bir damar genişletici olan CO_2'in kinetiklerini ekleyerek yeni bir model oluşturduk. Hemodinamik tepkinin zamansal karakteristiğini incelemek ve geriye doğru damar genişlemesi hipotezini test etmek amacıyla, yüksek çözünürlüklü bir görüntüleme yöntemi olan 2-ışın mikroskobu yardımıyla, Sprague-Dawley sıçanlarının somatosensöri kortekslerinden, önayak uyarımı esnasında, damar genişlemesini ölçtük. Sonuçlarımız, NO'in hemodinamik tepkiyi oluşturan asıl faktör olduğunu, CO_2'in ise tepkinin şeklini belirlemede etkili olduğunu göstermektedir. Model sonuçlarına göre, kan akışındaki artış, damardaki CO_2'in azalmasına ve böylece uyarı sonrası damar daralmasına sebebiyet vermektedir. Deney sonuçlarımızın istatistiksel analizleri geriye doğru damar genişlemesi hipotezini desteklemektedir. Model sonuçlarının deney sonuçlarıyla kıyaslanması tepki dinamiğini aydınlatmakta ve bunun yanısıra oksijen metabolizmasının artma ve azalma kinetiğinin saniyeler içinde gerçekleştiğini göstermektedir.

Anahtar Sözcükler: Sinir-damar etkileşimi, Nörojenik hipotez, Metabolik hipotez, Nitrik Oksit, Karbon dioksit, 2-ışın mikroskobu.

TABLE OF CONTENTS

LIST OF FIGURES

LIST OF TABLES

LIST OF SYMBOLS

a	Arteriole
c	Capillary
D	Diffusion rate
d	Diameter
d_{eff}	Effective diffusion distance
L	Length
M	M value
n	Neuron
P	Pressure
R	Radii
S	Signal
sm	Smooth muscle
v	Rate
v	Venule (subscript)
V	Volume
w/v	weight per volume
α	Solubility constant
α'	Laminar flow
β	Vascular compliance parameter
β'	Vascular compliance parameter
μ	Viscosity
τ	Decay constant

LIST OF ABBREVIATIONS

ANLS	Astrocytes Neuron Lactate Shuttle
ANOVA	Analysis of Variance
ADP	Adenosine Diphosphate
AMP	Adenosine Monophosphate
ATP	Adenosine Triphosphate
BOLD	Blood Oxygenation Level Dependent
CBF	Cerebral Blood Flow
CBV	Cerebral Blood Volume
$CMRO_2$	Cerebral Metabolic Rate of Oxygen
dHb	Deoxyhemoglobin
fMRI	functional Magnetic Resonance Imaging
GLC	Glucose
NAD^+	Nicotinamide Adenine Dinucleotide
NADH	reduced Nicotinamide Adenine Dinucleotide
NMDA	N-Methyl-D-Aspartate
NO	Nitric Oxide
NOS	Nitric Oxide Synthase
7-NI	7-nitroindazole
OCT	Optical Coherence Tomography
OISI	Optical Intrinsic Signal Imaging
pCO_2	partial pressure of CO_2
PEP	Phosphoenolpyruvate
PET	Positron Emission Tomography
PFK	Phosphofructokinase
PYR	Pyruvate
TCA	Tricarboxylic acid
HbT	Total hemoglobin

1. INTRODUCTION

1.1 Motivation and Objectives

The neurovascular coupling mechanism is intensely studied due to its vital role in brain health, both with the help of various imaging techniques and with the use of mathematical modeling tools. Any impairment in the coupling leads to ischemic lesions and even toxicity and many pathological disorders [4]. According to one of the two leading hypotheses on neurovascular coupling: the metabolic hypothesis, local CBF increase is a result of the vasodilators which are the metabolic products of neuronal activation [5]. Whereas according to the second hypothesis: the neurogenic hypothesis, local CBF is maintained via vasodilator neurotransmitters that are synaptic products released by the neurons during activation [5, 6]. Recent studies, on the other hand, have shown that the coexistence of both neurogenic and metabolic factors is needed to regulate cerebral perfusion [6, 7]. To this date, however, the problem is still being highly debated.

Another unresolved aspect of neurovascular coupling is whether the vessel dilation is controlled locally or remotely during functional activation. The association of the vessel dilation in the active region and the upstream pial artery dilation is also important because through such an association the flow increases in active regions but not in inactive regions vascularized by the same pial artery [4]. Although the retrograde dilation during functional activity in skeletal muscle is highly studied [8], this is not the case for the retrograde dilation in brain. The only study, to our knowledge, is by Chen et al. who measured the hemodynamic response in the rat somatosensory cortex during forepaw stimulation using optical coherence tomography (OCT) [9]. Any change in the OCT signals is correlated with the variations in scattering due to regional structural changes. The layer specific results they obtained during functional activity support retrograde dilation in the sensory cortex. However, supporting data, to our knowledge, has not been shown yet through the direct measurements of blood vessel

diameter changes located closer and further from the activation area.

Yet another highly debatable area related to metabolic changes during functional activity is the kinetics of $CMRO_2$. The estimations through PET, MR and optical imaging modalities are contradictory. While the PET study by Mintun et al showed a very slow onset kinetics with only 15 % increase after 25 minutes of stimulation [10], other recent works show a much faster increase in $CMRO_2$ [11, 12, 13, 14] reaching a steady state within a few seconds as a response to visual stimulation. The recent works do not relieve rather deepen the debate on this discrepancy.

1.2 Approach to the Problems

In this work, we aimed to answer the three unresolved problems related to neurovascular coupling mentioned above through both mathematical modeling approaches and experimental tools.

To compare the relative importance of the two neurovascular coupling hypotheses in producing changes in cerebral blood flow, blood volume, and oxygenation, we have constructed a biochemical model of neurovascular coupling which has the action potential firing frequency as an input. We have set CBF dependent on the neuronal signals resulting from synaptic activity, NO, and as a result of an energy metabolism product, CO_2. We have first tested the relative contributions of neurogenic and metabolic pathways for evoking changes in the CBF, blood oxygenation level dependent (BOLD) signal and partial pressure of CO_2 (pCO_2) and interpret our findings in the context of existing experimental findings described in the literature.

Secondly, we investigated the transient characteristics of the hemodynamic response both during and after the stimulus with a high-resolution imaging technique: 2-photon microscopy, which gives opportunity to measure the vessel diameter directly even in deep parts of the cortex. We have examined the effect of baseline vessel diameter and stimulus duration on the hemodynamic response *in vivo* during somatosensory

stimulus as well as during the post-stimulus period in Sprague Dawley rats. We analyzed the dilation transients so that we could be able obtain more information about the hemodynamic response, in particular, which characteristics of response depend on stimulus duration and which of them depends on vessel diameter or in other terms closeness to the activation area, since vessels having smaller diameters are located closer to the activation area. The latter is aimed to give insight to retrograde dilation. Following this, we compared our experimental findings related to hemodynamic response transients with our modeling results. We discussed how our model contributes to the explanation of the experimentally observed dynamics.

We, finally, investigated the $CMRO_2$ kinetics with the help of a comparison of our modeling and experimental findings. We compared the post-stimulus dilation undershoot and post-stimulus BOLD signal undershoot for this.

We hope this work will increase the current understanding of neurovascular coupling and help finding better treatment strategies for the disorders originating from an impairment in the coupling mechanism.

1.3 Thesis Outline

Following is the way the dissertation is organized:

Chapter 2 gives the background information on activity-metabolism coupling with emphasis on the various hypotheses on the cellular mechanism of coupling. It, then, continues with the neurovascular coupling hypotheses, basic vasodilators with a focus on NO and CO_2, hypotheses on the propagation of the coupling and the discrepancy in $CMRO_2$ kinetics in literature.

Chapter 3 describes the mathematical model and gives the necessary information on the differential equations and parameters used to be able to make duplication possible. The assumptions of the model are also introduced.

Chapter 4 is composed of the animal preparation protocol, the stimulus paradigm employed, the details of the imaging procedures with spectroscopic optical imaging and two-photon microscopy, and finally how the data is processed and analyzed.

Chapter 5 is the result section of the modeling part of the thesis. The results related to the contribution of metabolic and neurogenic mechanisms are given. The respond of the model to various stimulus durations are also provided.

Chapter 6 discusses the modeling results.

Chapter 7 is the results section of the experimental part of the thesis. The changes in dilation characteristics with changing baseline vessel diameter and stimulus duration are given with the corresponding statistical results. The section also includes the comparison of the model results with the experimental ones.

Chapter 8 discusses the experimental findings and the comparison of the model with experimental results.

Chapter 9 summarizes the major findings of the thesis and suggests possible future works.

2. BACKGROUND

The brain has little dissolved oxygen, thus to function properly, it strictly depends on a continuous oxygen supply through blood flow regulations [15]. In 1890, Roy and Sherrington discovered the coupling between local variations in neuronal activity and local cerebral blood flow increase [16], which is named as 'neurovascular coupling'. This discovery is confirmed later by many different studies and even lead to the development of various cerebral functional imaging modalities [5]. According to Roy and Sherrington's proposal, substances released by activated neurons are responsible for the relaxation of the smooth muscles around the blood vessels [17]. Although the discovery of neurovascular coupling goes back to a century ago, the substances responsible for the coupling, and by which mechanism they lead to coupling are still a subject of debate. We give a theoretical background on the activity-metabolism and neurovascular coupling hypotheses at hand. We will continue with the introduction to the discussion on how hemodynamic response, once produced, propagates. Finally, we will introduce a yet unresolved problem in literature: discrepancy in the experimental results on the kinetics of cerebral metabolic rate of oxygen, the final question we will try to seek an answer with the comparison of our modeling and experimental approaches.

2.1 Activity-Metabolism Coupling in Brain

Glucose, being the main energy substrate of the brain, has several fates depending on the cellular conditions. Under anaerobic conditions or low oxidation rates, pyruvate, the end product of glycolysis (the metabolism of glucose to pyruvate), is converted into lactate in cytoplasm giving two adenosine triphosphates (ATP) as an outcome [18]. Under aerobic conditions, on the other hand, glycolysis end product pyruvate enters tricarboxylic acid (TCA) cycle in mitochondria, and with the help of oxidation-reduction reactions, it is totally oxidized to CO_2 and H_2O and produces ATP [18]. A third way, glucose is consumed is the pentose phosphate pathway where

NADPH, energy in the form of reducing equivalents, is obtained [18].

The [14C] deoxyglucose method developed by Sokoloff and friends in 1977 provided the opportunity to measure glucose consumption rate in brain [19]. Its major contribution to neuroscience was the fact that neuronal activity leads to increases in glucose consumption thus increases in energy metabolism [20]. It is stated for many years that the resting energy requirements and the increases in energy metabolism during functional activity of the mammalian brain are obtained entirely through ATP generation by the oxidative phosphorylation of glucose [15]. However, the low oxygen-glucose ratio and the existence of lactate transporters in the brain endothelium suggest that glycolysis also takes place during functional activity though its contribution is small [21].

The rate of oxygen consumption increase varies with stimulus type. Gjedde et al. classified the various stimulus types as primary and complex according to their energy requirements [21]. While complex stimuli like a checkerboard containing chromatic patterns increase oxygen consumption [22], a simple photic stimulus produced a much less increase in oxygen consumption [23]. The degree of change in energy metabolism is directly related to degree of postsynaptic depolarization during functional activity.

2.1.1 The Cellular Basis of Activity-Metabolism Coupling

Attwell and Laughlin estimated the energy expenditure related to various functions of grey matter of the rodent brain using published experimental data [24]. Their findings suggest that most of the energy is used during the restoration of the ion movements generated by action potentials (47 %) and postsynaptic potentials (37 %) in neural cells. These are followed by neuronal and glial resting potentials (13 %), presynaptic calcium entry and neurotransmitter recycling (3 %) and calcium transients in spines and vesicle recycling ($<$1%). The maintenance of the electrochemical gradients is obtained through pumping activities of the specific ATP-consuming enzymes across the membrane, a very common one being Na^+/K^+-ATPase [18].

2.1.2 Na^+/K^+-ATPase

Most of the energy produced by neurons is consumed during action potentials and postsynaptic potentials to restore the resting membrane potentials. Maintenance of low intracellular Na^+ activity is a basic feature of neurons. During action potentials or postsynaptic potentials, however, Na^+ influxes through cell membrane and increases intracellular Na^+ levels. To restore the intracellular Na^+ levels, Na^+ gradient is obtained by Na^+/K^+-ATPase which is an enzyme that hydrolyzes ATP to exchange 3 intracellular Na^+ for 2 extracellular K^+ [25]. The mechanism by which Na^+/K^+-ATPase cause higher levels of glucose consumption is first introduced by Proverbio and Hoffman in 1977 [26]. The ATP, hydrolyzed by Na^+/K^+-ATPase, is also a negative modulator of phosphofructokinase (PFK), the rate-limiting enzyme of glycolysis. Hence a decrease in ATP through hydrolization by the pump stimulates the PFK activity hence glycolysis [18].

2.1.3 Another Possible Activity-Metabolism Related Mechanism: Glutamate-Induced Glycolysis in Astrocytes during Physiological Activation.

Glutamate-glutamine cycle was first introduced by Van den Berg and Garfinkel in 1971 [27]. The cycle can be briefly described with the following sequence of events: 1) glutamate, a well-known excitatory neurotransmitter, is released from presynaptic terminals during neuronal activity, 2) the glutamate in the synaptic cleft is then taken up by the astrocytes nearby, 3) glutamate is converted into glutamine, a non-neuroexcitatory amino acid, by glutamine synthtase in astrocytes, 4) finally, the glutamine released by astrocytes is taken up by the neurons for further processing into glutamate [28].

Pellerin and Magistretti proposed a new mechanism which couples glutamate-glutamine cycle to glucose consumption in astrocytes [29]. In their work, they have shown that glutamate stimulates glucose consumption and lactate production in astrocytes [29]. They suggested, based on their experimental findings, that the need for ATP

for the conversion of glutamate into glutamine and to reestablish Na^+ gradients, the glycolytic pathway in the astrocytes is triggered [30]. It is further suggested that the changes in glucose metabolism are mainly linked to the cycling of neurotransmitters [30, 31], a hypothesis which needs further experimental support, since it is reported that only 2 % of brain energy supports glutamate recycling in glia [24].

Pellerin and Magistretti further proposed astrocytes-neuron lactate shuttle (ANLS) hypothesis which claims that the lactate released by astrocytes are partly taken up by the neurons and processed in oxidative phosphorylation [29]. The hypothesis, however, is still being debated. A supporting in vitro work was performed by Pellerin and Magistretti, in which they showed that cultured astrocytes, when exposed to glutamate, release lactate [29]. Moreover, when primary neuronal cultures are exposed to both lactate and glucose, they prefer lactate as their oxidative substrate [32]. A similar trafficking is proposed between Müller glial cells and photoreceptors from retina [33].

On the other hand, there are several works claiming that glucose is the major energy substrate of neurons during neuronal activity thus challenging this hypothesis. One of the studies is of Bak et al. who showed that glucose is necessary as a substrate during synaptic activity in cultured glutamatergic neurons [34]. Moreover, Mangia et al. showed an early lactate decrease during stimulus; as opposed to a lactate overproduction which would be expected if ANLS hypothesis holds [35]. Though it is used for ANLS hypothesis, Kasischke's work on hippocampal slices also supports the work by Mangia et al [36]. They observed an early reduced nicotinamide adenine dinucleotide (NADH) decrease in neurons and a late NADH increase in astrocytes, supporting the idea that neuronal oxidative metabolism takes place before astrocytic glycolysis. Moreover, the lactate produced during neuronal activity is detected in brain venous blood for many years [15]. Gjedde et al.'s have hypothesized using *in vivo* data that no ANLS takes place during either simple neuronal stimulus or during complex neuronal activity due to the clearance of lactate produced by astrocytes by the wash-out effect of cerebral blood flow [21]. Simpson et al. even claimed that the neurons are the responsible parties for the lactate production during neuronal activity [37].

2.2 Neurovascular Coupling Hypotheses

2.2.1 Two Hypotheses of Neurovascular Coupling

There are basically two hypotheses of neurovascular coupling based on various couplings. The first hypothesis, 'the metabolic hypothesis' is that vasodilatation is mediated through metabolic products of increased energy consumption e.g. H^+, lactate, CO_2 and adenosine during functional activation [38]. This hypothesis is based on the coupling between neuronal activity and metabolism: so called 'activity-metabolism coupling', and the coupling between metabolism and flow: so called 'flow-metabolism coupling' [39]. Roy and Sherrington were the firsts to claim that these energy-consumption related regulatory substances are oxygen and glucose [16]. Changes in metabolic demand and changes in cerebral blood flow are shown to be very well correlated during rest [40]. However the coupling between the two is not as clear during functional activation. Regional uncoupling is found between $CMRO_2$ and CBF during somatosensory stimulation: increase in CBF being much more than the increase in $CMRO_2$ [40]. So, they proposed that the mechanism by which CBF is regulated is independent of $CMRO_2$ [40, 23]. Moreover, unless being severe (below 40 mmHg), arterial hypoxia does not lead to a considerable CBF increase [41] and the modulation of arterial pressure of oxygen and glycemia do not affect the CBF increase during whisker deflection [42], supporting a mechanism independent from any changes in energy substrates i.e. oxygen and glucose for the regulation of CBF. Lu et al. showed that there is a sustained post-stimulus elevation of $CMRO_2$ after blood volume recovery [38] supporting the idea that the production of metabolites is not sufficient to account for the CBF increase during activation. The role of 'local' CO_2, another energy metabolism related molecule, however, has not been determined so far, although the effect of any change in CO_2 on cerebral blood flow is well established.

The second hypothesis 'the neurogenic hypothesis', on the other hand, claims that vasodilatation is caused by an increase in neurotransmitter release, which binds to neurons and triggers formation of nitric oxide, a well know vasodilator, and other mediators [38]. This second hypothesis is based on the coupling between neuronal

activity and flow, so called 'activation-flow coupling' [39].

However, recent studies claim that the coexistence of both neurogenic and metabolic factors is needed to regulate cerebral perfusion [6, 7], although it is not proved by either an experimental or a modeling approach. Hence there is a need in comparing the relative importance of these two neurovascular coupling hypotheses in producing changes in cerebral blood flow, blood volume, and oxygenation. We will now introduce the research in literature on basic vasoactive mediators and their possible role in hemodynamic response. The ones stressed in our modeling approach namely NO and CO_2 are introduced in more detail in the following sections.

2.2.2 Basic Vasoactive Mediators

K^+, lactate, adenosine and H^+ are among the vasoactive metabolic products of neuronal activity [18]. K^+ is a vasoactive mediator of neurovascular coupling. K^+ siphoning is one of the hypotheses trying to describe its role in coupling [43]. Briefly, the hypothesis implies that the K^+ released by neurons during functional activity is taken up by glial cells. Glial cells, then, release K^+ into the area between the astrocytic end-feet and the smooth muscle cells on the walls of arterioles [43]. The resultant hemodynamic response depends on K^+ concentration: high K^+ release leads to vasoconstriction, while a slight increase leads to dilation [17]. Metea et al.'s in vitro experiment, on the other hand, has shown that K^+ siphoning does not contribute to neurovascular coupling [44]. Rather the role of glia on neurovascular coupling is through the induction of vasoactive arachidonic acid metabolites: epoxyeicosatrienoic acids and 20-hydroxyeicosatetraenoic acid [44]. The type of vasomotor response: dilation/constriction depends on the nitric oxide levels. Moreover, extracellular K^+ concentration returns to its basal levels in 30 to 40 seconds after stimulus which is longer than the vascular return time [45]. This finding suggests that K^+ does not contribute to vascular response during post-stimulus period [38].

Lactate as a metabolic product can also be considered as a vasodilatory neu-

rovascular mediator through increasing H^+ concentration, however its increase during neuronal activity is rather low and transient to fully accomplish this task [4]. Adenosine is also a mediator of neurovascular coupling. The dilatory mechanism of adenosine is investigated by Newman in detail [46]. Glial cells release ATP during activation which is then hydrolyzed by a variety of enzymes into adenosine which causes the dilation of arterioles mainly through A_{2A} receptors [17]. However, the delay in their formation and the fact that they can diffuse only to a certain distance show that they are not sufficient to explain the whole hemodynamic response [18]. Moreover the release of H^+ and adenosine only takes place when there is a mismatch between oxygen delivery and consumption [47]. Increases in extracellular H^+ during functional activity particularly, as in the case of K^+, is not sufficient to account for the hemodynamic response [48].

In the following two sections, two well-known vasodilators, namely CO_2 and NO, and the mechanism by which they lead to dilation will be introduced in detail.

2.2.3 The Mechanism by which CO_2 Mediates Dilation

The CO_2 is a product of oxidative phosphorylation whose dilatory effect on blood vessels is very well established. Kety and Schmidt investigated the effects of hypercapnia -high levels of CO_2 in blood- and hypocapnia -low levels of CO_2 in blood- on cerebral blood flow in 1948 [1], by using their novel method of measuring CBF by inhalation of an inert gas: nitrous oxide [1]. They have shown that hypercapnia produced by the inhalation of 5-7 % CO_2 resulted in an increase in CBF by 75 %, while hypocapnia lead to a reduction in CBF levels. The local effect of CO_2 is also studied. Kontos et al. investigated the effects of hypercapnic acidosis and hypocapnic alkalosis on pial arterioles in anesthetized rats [49]. They found that local application of hypercapnic acidosis and hypocapnic alkalosis dilated and constricted the vessels in the exposed area respectively.

The sensitivity of CBF on CO_2 concentration is used as a tool to estimate the cerebral perfusion reserves [47]. Besides giving insight to enormous number of research

studies on brain hemodynamics, it also has a prognostic value in clinics. For example an impaired reserve is an implication of already dilated resistance vessels as in the case of carotid stenosis [47].

How CO_2 affects vessels is also investigated. Two basic mechanisms are suggested: either CO_2 directly acts on the membrane or the intracellular structures of the vascular smooth muscle cells, or it acts on cells other than smooth muscle cells, which then produce vasoactive substances to change the vascular mode [49]. The former hypothesis is found to be the most likely mechanism [49]. The way by which CO_2 changes vascular tone is studied by Chen and Anderson [50]. They have found that the effect of CO_2 on the contractility of pericytes is mediated by its influence on the pH. In addition to direct pH effects, other CO_2 related mechanism might also play a role in dilation [47]. In this secondary mechanism, prostaglandin, a vasoactive substance and arachidonic acid were suggested to mediate CO_2 dependent dilation [51].

The effect of CO_2 on cerebrovasculature is also studied using mathematical modeling tools. Ursino et al. constructed a hemodynamic model composed of electrical circuit equivalents in order to simulate the changes in cerebral hemodynamics and intracranial pressure as a response to mean systemic arterial pressure and arterial CO_2 pressure changes [52, 53]. The arterial CO_2 pressure is an input to the model. With a similar approach, Payne predicts the vascular response to arterial blood pressure, neuronal stimulus and arterial CO_2 concentration [54]. A non-linear model by Zheng et al. is an extension of the original Balloon/Windkessel model [55, 56, 57] to describe the coupling between flow and oxygen delivery, which also gives opportunity to determine the time series of $CMRO_2$ under CO_2 challenges [58]. Above models, however, do not include the effect of any possible contribution of local CO_2 production; rather they give arterial CO_2 change as an input to the model, mimicking hypercapnia induced by systemic inhalation.

Although blood pCO_2 remains unchanged during functional activity or arterial blood pressure changes, local pCO_2 at the site of activation may change [49]. However, if CO_2 is to be a regulator of vascular mode during activation, it should have a strong

action on vessels [49]. There are many studies on CO_2 effect on vascular mode through systemic inhalation or local application. The effect of locally produced CO_2 due to the increases in energy metabolism as a response to neuronal activity, on the other hand, has not been revealed yet to our knowledge.

2.2.4 The mechanism by which NO Mediates Dilation

Nitric oxide plays significant roles in the regulation of cerebral blood flow and cell viability and in the protection against pathogenic conditions such as Alzheimer's disease, Huntington's disease, seizures, and migraine [59]. It has been first discovered by Furchgott and Zawadski as the endothelial-derived-relaxing-factor in 1980 [60]. Having properties such as high diffusibility and short half-life makes this molecule a powerful candidate for being the link between neuronal activity and local blood flow [5]. NO is synthesized by nitric oxide synthase (NOS) which has an endothelial form: eNOS, a neuronal form: nNOS and an inducible form: iNOS. The neuronal form is localized next to the cerebral vessels [39], and a study on rat cerebral cortex has shown that it is enriched in neuronal NOS [61].

The NO type responsible for the increase in CBF during functional activity is not endothelial origin [5]. Confirming this, Ayata et al. showed that eNOS knocked-out mice behaved like the control group in giving hemodynamic response to stimuli [62]. This brings the conclusion that functional activity related CBF changes are mediated by neuronal NO. The vasodilatory role of neuronal nitric oxide during neuronal activity has been shown by many studies. *in vivo* studies by Buerk et al showed that NO has vasodilatory effects during flicker stimuli in cat optic nerve [63] and during forepaw stimuli in rat somatosensory areas [64]. The effect of neuronal NO on CBF is also studied by various groups using 7-nitroindazole (7-NI), a specific inhibitor for neuronal NOS. They have found that 7-NI significantly diminishes the CBF increase during functional activation [65, 66, 67, 68]. The effect of nitric oxide is also shown in cerebellar cortex [69]. Moreover its role in hemodynamic response in cerebellum is dominant among various factors [67, 70].

During neuronal activity, Ca^{2+} influxes into the cell by the activation of glutamate receptors, mainly the N-methyl-D-aspartate (NMDA) receptors in the post-synaptic neurons [71, 72]. Ca^{2+} increases in the cytosol, and by forming a complex with calmodulin, activates neuronal NOS, which then leads to the production of NO from the amino acid L-arginine [73, 74]. The return of Ca^{2+} concentration to its resting levels acts as a switch that turns the enzyme off [75]. The NO produced by the functional activity, then, diffuses to the surrounding extracellular medium and arterioles and lead to dilation [74]. NO relaxes vascular smooth muscle through a cyclic GMP-dependent mechanism [76]. Increase in NO concentration leads to increases in intracellular cyclic GMP concentrations in vascular smooth muscle cells [71]. However, the rest of the mechanism which leads to dilation is not fully understood. The various possible mechanisms are listed in a review by Esplugues et al. as direct channel gating with the opening of inward Ca^{2+} and Na^{+} channels, activation of cyclic GMP-dependent kinases, actions related to cyclic adenosine diphosphate (ADP) ribose, and interactions with cyclic adenosine monophosphate (AMP), all of which results in a reduction in intracellular Ca^{2+} concentrations in smooth muscle cells leading dilation [75].

Mathematical modeling approach is applied to further understand especially the biotransport of nitric oxide. The main question is that how NO can be a potent dilator, while being strongly scavenged by hemoglobin (for a detailed review please see Buerk, 2001 [77]). A non steady-state model of nitric oxide diffusion in vascular smooth muscle cells by Seraya and Nartsissov is an example for the transport models of NO [78]. The main results of the model are the observation of dilation even a short time after NO production and the dependency of nitric oxide effect on NO concentration gradient and the diameter of the vessel. The co-transport of NO and oxygen in a capillary-perfused tissue is also investigated with modeling tools [79]. Among the model predictions is that when capillaries are included, the NO in the arteriolar wall significantly increases. Beside these modeling approaches, there is still a need for a model which can predict how NO release is triggered during neuronal activity and how it controls vascular smooth muscle tone and blood flow.

2.2.5 The Common Effect of CO_2 and NO

Previous research on rats suggests that inhibition of nitric oxide synthase reduces the CBF response to hypercapnia [80], on the other hand, more recent research on humans found no significant change in CBF response to hypercapnia under NOS inhibitors [81]. Moreover, Ances et al. measured CBF changes as a response to forepaw stimulus at various blood CO_2 concentrations [82]. They found that the absolute magnitude of CBF changes is independent of CO_2 concentrations, which also suggests a NO related dilation mechanism independent of the CO_2 levels.

2.3 Mathematical Modeling as a Tool to Understand Brain Hemodynamics

Brain hemodynamics is intensely studied using different neuroimaging modalities such as fMRI, PET and optical imaging. Each one of these modalities provides valuable insight into specific components of neurovascular coupling. Recent work in neuroimaging studies demonstrates that not only integration of multiple neuroimaging modalities is required, but that mathematical modeling is necessary to understand the complex physiology underlying neurovascular coupling. There are numerous models aiming to explain either the vascular or the neurometabolic response to brain activation. The Balloon and Windkessel models are among the ones describing the vascular response. According to the Balloon model, the venous compartment expands as a result of the output of the capillary bed [56]. The Windkessel model extends the balloon model to incorporate vascular compliance [57]. A neurometabolic model that couples brain electrical activity and energy metabolism via the Na^+-K^+ pump and mitochondrial respiration was developed by Aubert and Costalat [83]. They recently extended that model by adding an astrocytic compartment [84]. There exist models that combine the vascular and metabolic compartments to investigate how cerebral blood flow is controlled via metabolic and neurogenic pathways. Banaji's model is a good example that focuses on autoregulation of the blood vessels via different feedback mechanisms

[85]. While these are just a few of the numerous models described in the literature, in general there is a need for a model which describes cerebral blood flow in terms of both neurogenic and metabolic mediators that are directly related to the neuronal stimulus as an input to the model.

2.4 The Propagation of the Hemodynamic Response

Another unresolved aspect of neurovascular coupling is whether the vessel dilation controlled locally or remotely during functional activation. The hemodynamic response of the microcirculation in the activated area should be accompanied by the dilation of the upstream arterioles in order to be sufficient for the metabolic demands during functional activation. The association of the vessel dilation in the active region and the upstream pial artery dilation is also important because through such an association the flow increases in active regions but not in inactive regions vascularized by the same pial artery [4]. As early as 1919, it is proposed by Krogh that the capillary perfusion during functional activity is regulated locally [86] in agreement with the rapid onset of functional vasodilation. In 1970, Duling and Berne applied acetylcholine to the arteriole of hamster cheek pouch of the golden hamster and observed that dilation spread rapidly upstream and downstream, and proposed that this dilation takes role in integrating the dilation of terminal arterioles to the upstream arteries so called 'retrograde dilation' [87]. The conducted vasodilation is also shown in rat cerebral arterioles [88]. In 1959, Hilton proposed that the dilation is conducted through the smooth muscle cells of the vessel wall independent of any neural mechanism [89]. Confirming this, an electrical coupling between the capillaries and arterioles is shown to exist in hamster cheek pouch [90]. Moreover, Sokoya et al. found that cerebral endothelial cells and smooth muscle cells are connected by gap junctions through which they propagate dilation from the site of activation to upstream vessels [91]. Moreover the local vasodilation may also increase flow velocity in upstream arteries through flow mediated vasodilation [17]. The increase in upstream arteries then enhances the increase in perfusion further [92]. Briefly, the vasoactive substances lead to dilation of the vessels in the vicinity of the activated area, and this dilation is conducted or propagated to the

upstream feeding arterioles and arteries through the gap junctions between the smooth muscle cells located at the walls of the vessels.

Although the retrograde dilation during functional activity in skeletal muscle is highly studied [8], this is not the case for the retrograde dilation in brain. Iadecola et al. studied cerebellar cortex to investigate retrograde dilation during functional activity. They have observed that the stimulation of parallel fibers produces vasodilation both at the activated area and at the upstream arterioles feeding it [93]. They concluded that the upstream dilation is due to the propagation of the dilation at the site of activation since no neuronal activity is observed in the upstream regions. Chen et al. measured the hemodynamic response in the rat somatosensory cortex during forepaw stimulation using optical coherence tomography [9].The layer specific results they obtained during functional activity support retrograde dilation in the sensory cortex.

2.5 An Unresolved problem: Different $CMRO_2$ Kinetics

PET, fMRI and optical imaging modalities differ in the estimated $CMRO_2$ onset kinetics. This leads to different flow-consumption kinetics during the onset of the stimulus. The difference in $CMRO_2$ kinetics can be understood by looking at specific studies. A PET study by Mintun et al showed a 4.7 % increase in $CMRO_2$ 60 s after the stimulus onset, while this value reaches 15 % after 25 minutes of stimulation [10]. A recent work from Lin et al. also obtained slow $CMRO_2$ onset kinetics using fMRI [94]. The work of Prichard et al. confirms this slow increase in $CMRO_2$, showing a slow lactate decay after the onset of photic stimulation [95]. In contrary, other recent works show a much faster increase in $CMRO_2$ [11, 12, 13, 14]. For example; Wu et al. calculated the $CMRO_2$ from CBF and BOLD signals using a biophysical model. They obtained a $CMRO_2$ increase, reaching a steady state within a few seconds as a response to visual stimulation. This is also supported by two recent studies, which use pharmacological agents to eliminate the blood flow response, and measure the BOLD signal in response to stimulation as an indicative of $CMRO_2$. Time to peak values in these studies are around 10 seconds, supporting a faster $CMRO_2$ onset kinetics [96, 97].

3. METHODS - MATHEMATICAL MODEL

3.1 Model Description

Our model is designed to explore the relative importance of two neurovascular coupling mechanisms in producing a blood flow response given changes in the frequency of action potentials: one of metabolic origin and the other neurogenic. The metabolic mechanism is based on the product of oxidative phosphorylation, carbon dioxide; whereas the neurogenic mechanism is based on nitric oxide, a synaptic activity product (Figure 3.1). These two factors diffuse to the extracellular matrix and then to blood vessels and produce vasodilation in the arterioles giving rise to changes in regional CBF and the BOLD signal.

The model has one input which is the frequency of action potentials. This can be kept constant or can be expressed as a time-dependent function throughout the stimulus duration. This frequency modulates the cell membrane potential by changing the flux of sodium and calcium ions across the membrane resulting in energy-product related and synaptic activity related vasodilation respectively. The sodium entry into the cell during an action potential increases the intra-cellular sodium concentration, thus increasing the Na^+-K^+ pump rate and consumption of ATP. The ATP supply for Na^+-K^+ pump comes from the phosphocreatine buffer, glycolysis, and mitochondrial respiration. Glucose (GLC) is delivered to the tissue by the vessels, and it turns into pyruvate (PYR) by passing through the glycolysis intermediary steps: glyceraldehyde-3-phosphate (GAP) and phosphoenolpyruvate (PEP). After this point PYR either goes to mitochondria and starts oxidative phosphorylation via aerobic respiration, or it turns into lactate (LAC) via anaerobic respiration. During these processes, there is a continuous electron transfer between NAD and NADH, and a phosphate transfer between ATP and adenosine diphosphate (ADP).

The equations describing sodium membrane transport, the Na^+-K^+ pump, neu-

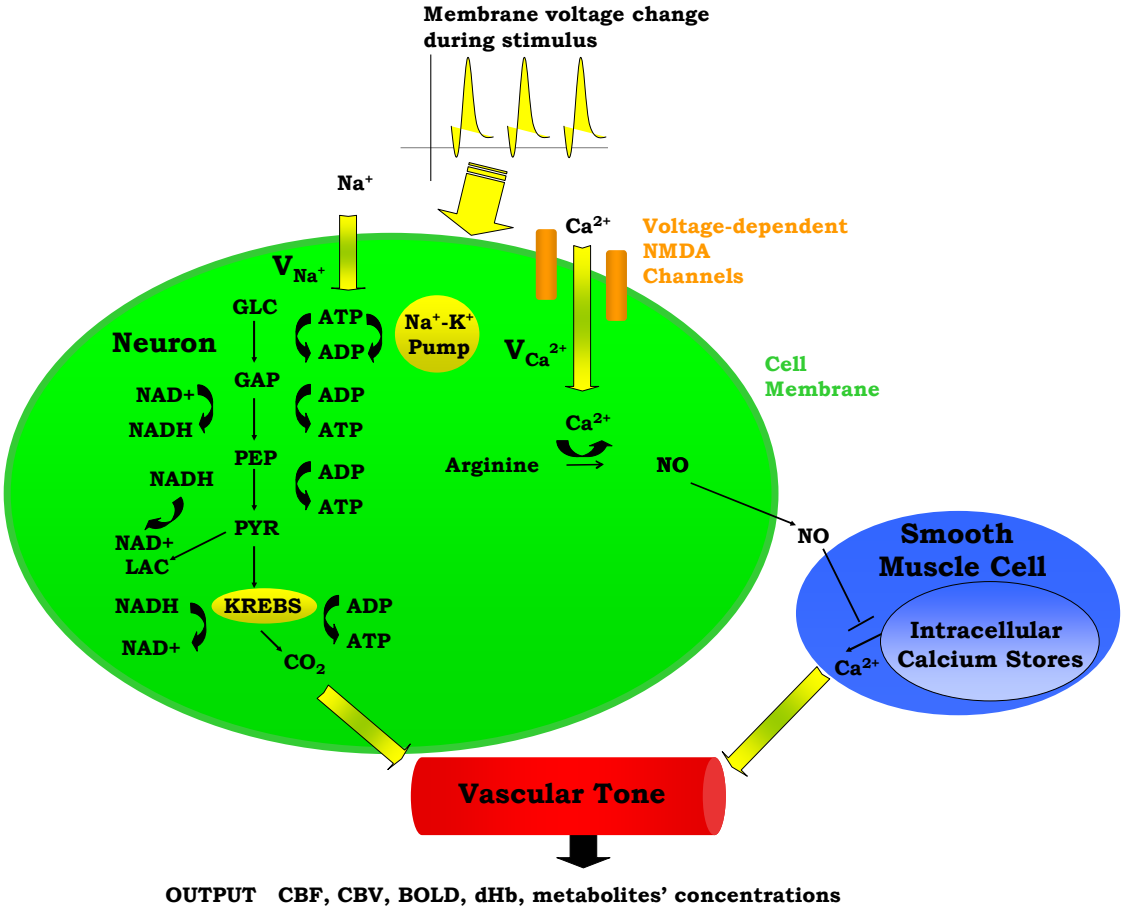

Figure 3.1 A schematic representation of the proposed model. ADP: Adenosine diphosphate, AP: action potential, ATP: adenosine triphosphate, BOLD: blood oxygenation level-dependent, Ca^{+2}: calcium, CBF: cerebral blood flow, CBV: cerebral blood volume, CO_2: carbon dioxide, dHb: deoxyhemoglobin, GAP: glyceraldehyde-3-phosphate, GLC: glucose, K^+: potassium, LAC: lactate, Na^+: sodium, NAD^+: nicotinamide adenine dinucleotide, NADH: reduced nicotinamide adenine dinucleotide, NO: nitric oxide, PEP: phosphoenolpyruvate, PYR: pyruvate.

ronal energy metabolism (phosphocreatine buffer, glycolysis), and blood-brain-barrier exchange reactions are provided by Aubert and Costalat [83], and the equations for NADH kinetics and mitochondrial respiration are provided by Aubert et al. [98]. The vasodilator carbon dioxide is produced as a result of oxidative phosphorylation. The other vasodilator nitric oxide, NO, is produced as a result of Ca^{2+} entry into the neuron which activates NO production. NO then diffuses to and enters the smooth muscle cells around the arterioles. It then inhibits Ca^{2+} efflux from internal Ca^{2+} sources in these cells and so leads to vasodilation [99]. CBF is assumed to be dependant only on arteriolar diameter changes as given by Poiseuille's equation, and the pressure drop between the two ends of the vessel is assumed to be constant. The BOLD signal is then derived from $CMRO_2$ and CBF using Davis' BOLD equation [11].

In the next subsections, we provide details of each step in our model. The initial conditions for the new variables added to Aubert's model in this work are presented in Table 3.1, and all parameters are defined in Tables 3.2 and 3.3. Unless otherwise stated, concentrations of metabolites are in mmol/L. The reaction rates are in mmol/L s. The subscripts within the tables and the text are a: arteriole, n: neuron, v: venule, c: capillary (in our case capillary stands for pre-capillary arteriole), sm: smooth muscle.

Table 3.1
Initial values for the variables of the model.

	Concentration
Intracellular carbon dioxide (CO_{2n})	1.25 mM
Capillary carbon dioxide (CO_{2c})	1.23 mM
Intracellular calcium (Ca^{+2n})	6937 nM
Intracellular nitric oxide (NO_{sm})	0.18 nM
Neuronal nitric oxide (NO_n)	0.21 nM

3.2 Action Potentials Modulate Intra-cellular Na^+ and Ca^{2+} Concentrations

Our model uses action potential frequency as an input. In our model, the action potential frequency is assumed to be almost 0 before and after the stimulus and taken as 150 Hz during the stimulus. We have fit a gaussian function to a generic action potential [112] to obtain the membrane voltage changes as a function of time,

$$\tilde{V}(t) = a_1 \times \exp\left(-\left(\frac{t-b_1}{c_1}\right)^2\right) + a_2 \times \exp\left(-\left(\frac{t-b_2}{c_2}\right)^2\right)$$

$$+\mathrm{a}_3 \times \exp\left(-\left(\tfrac{t-b_3}{c_3}\right)^2\right) + a_4 \times \exp\left(-\left(\tfrac{t-b_4}{c_4}\right)^2\right) + a_5 \times \exp\left(-\left(\tfrac{t-b_5}{c_5}\right)^2\right) \quad (3.1)$$

where $\tilde{V}(t)$ is the voltage in mV as a function of time t and the remaining parameters are specified in Table 3.2. The voltage change for a train of action potentials is obtained by convolving Eq. 3.2 with the sequence of action potentials ($S(t)$) as

$$V(t) = \int \tilde{V}(t')S(t-t')dt \quad (3.2)$$

where $S(t)$ is equal to 0 unless t is at the onset of an action potential such that $S(t) = \sum \delta(t - t_n)$. For example, for action potentials arriving at a frequency of 100 Hz, $t_n = n\Delta t$, where Δt= 10 ms.

This voltage change is then used to obtain the voltage-dependent Na^+ and Ca^{2+} channel activations. The Na^+ influx ($v_{Na^+}(t)$) as a function of voltage and time is obtained by the Hodgkin-Huxley equations [113]. The current calculated using Hodgkin-Huxley equations is then converted from $\mu A/cm^2$ to mmol/Ls considering a 5 μm-radii spherical cell.

Calcium influx in the neuron is mediated through N-Methyl-D-Aspartate Receptor (NMDAR) channels that are voltage dependent [114] (Eq. (3a)). This influx, the rate of Ca^{2+} concentration change in the neuron ($v_{Ca^{+2},n}$), is given as a product of the fraction of NMDARs that move from the closed to open state after each presynaptic

action potential, the peak NMDA receptor conductance and the membrane potential (please see [114] for a detailed description of the equations and parameters).

The rate of intracellular sodium concentration change ($v_{Na^+}(t)$), is used as an input to the metabolic rate equations described in Section 3. The rate of intracellular calcium concentration change ($Ca^{+2,n}$), is used in the production of NO as described in Section 5.

3.3 A Brief Description of Aubert and Costalat's Model of Stimulus Induced Changes in Oxygen Consumption

The portion of Aubert and Costalat's model [83] that we utilize here couples ionic current (Na^+ ion flux) to brain energy metabolism (glycolysis, mitochondrial respiration and the phosphocreatine buffer). An increase in intracellular Na^+ activates the Na^+-K^+ pump and consumes more ATP. To compensate for the ATP decrease, the cell produces ATP through glycolysis, mitochondrial respiration and the phosphocreatine buffer. The following equation from the work of Aubert et al. [98], which is based on the respiratory chain equation from Holzhütter et al. [115] is used to describe the $CMRO_2$ in the model. The description and values of the parameters V, nop, Km_{ADP}, kr, phi, phi_0, H, Hm and nr can be found in [98].

$$CMRO_2 = V\left(\frac{ADP^{nop}}{ADP^{nop} + Km_{ADP}}\right)\left(\frac{kr}{1+phi}\right)\left(\frac{O_{2n}}{O_{2n} + qr.phi}\right) \tag{3.3}$$

$$phi = phi_0\left(\frac{NAD}{NADH}\right)^{0.5} \tag{3.4}$$

$$phi_0 = pr\left(\frac{H}{H_m}\right)^{nr/2} \tag{3.5}$$

This oxygen consumption modulates the oxygen concentration in the tissue, altering the concentration gradient with respect to the blood vessel (Eq. (28) from [83]), thus changing the rate of oxygen extraction from the vessel (Eq. (43) from [83]).

3.4 CO_2 Kinetics

The carbon dioxide concentration in the neuron increases with mitochondrial respiration and decreases with CO_2 diffusion from the neuron to the precapillary arterioles via the concentration gradient,

$$\frac{dCO_2}{dt} = n_{Aero} v_{mito} - \frac{V_c}{V_n} v_{CO_2 nc} \tag{3.6}$$

The mitochondrial respiration rate (v_{mito}) is given by Eq.(23) from [98]. According to the brain tissue compartmentalization assumption of Aubert and Costalat, Vc and Vn are the volume fractions of the precapillary arterioles and neurons in the brain respectively, and naero is the stoichiometric constant. The rate of CO_2 diffusion from the neuron to the precapillary arterioles ($v_{CO_{2nc}}$) is given by

$$v_{CO_2 nc} = D_{new,CO_2} \frac{1}{V_c} (CO_{2n} - CO_{2c}) \tag{3.7}$$

$$D_{new,CO_2} = D_{CO_2} / d_{eff}^2 \tag{3.8}$$

where D_{new,CO_2} is the effective diffusion rate depending on the CO_2 diffusion coefficient (D_{CO_2}) and effective distance that CO_2 diffuses (d_{eff}). CO_{2n} is the concentration of CO_2 in the neuron and CO_{2c} is the concentration of CO_2 in the precapillary arterioles.

This CO_2 diffusion increases CO_2 concentration in the precapillary arterioles that is cleared by the in-flowing blood from the artery,

$$\frac{dCO_2}{dt} = v_{CO_2,nc} - v_{CO_2,ca} \tag{3.9}$$

The rate of change of CO_2 in the precapillary arterioles due to the flowing blood is given by

$$v_{CO_2,ca} = 2F_{in} \frac{1}{V_c} (CO_{2c} - CO_{2a}) \tag{3.10}$$

where CO_{2a} is the concentration of CO_2 in the upstream artery.

3.5 $Ca^{2+}$and NO Kinetics

Calcium concentration in the neuron varies with the difference between calcium influx into the cell and the calcium decay,

$$\frac{dCa_n^{+2}}{dt} = v_{Ca^{2+}} - v_{Ca_{decay}^{+2}} \tag{3.11}$$

Calcium influx ($v_{Ca^{2+}}$) is described in Section 3.2. The calcium decay rate ($v_{Ca_{decay}^{+2}}$) is given by Majewska [102],

$$v_{Ca_{decay}^{+2}} = \frac{1}{\tau_{Ca^{2+}}} \times Ca_n^{2+} \tag{3.12}$$

where Ca_n^{2+} is the calcium concentration in the neuron and $\tau_{Ca^{2+}}$ is the decay time constant.

NO concentration in the neuron is determined by the rate of NO production ($v_{NO,n}$), the diffusion of NO from the neuron to smooth muscle ($v_{NO,sm}$), and the decay of NO in the neuron ($v_{NOdecay,n}$):

$$\frac{dNO_n}{dt} = v_{NO,n} - v_{NO,sm} - v_{NOdecay,n} \tag{3.13}$$

NO production is related to neuronal calcium concentration by Takahashi and Mendelsohn [116], assuming that the maximum neuronal NO release is obtained during the maximal activation of nitric oxide synthase [117],

$$v_{NO,n} = 0.0053 \left(Ca^{2+}\right)^{0.4066} \tag{3.14}$$

The NO produced in the neuron then diffuses to the smooth muscle cells around arterioles

$$v_{NO,sm} = D_{new,NO} \left(NO_n - NO_{sm}\right) \tag{3.15}$$

$$D_{new,NO} = D_{NO}/d_{eff}^2 \tag{3.16}$$

where $D_{new,NO}$ is the effective diffusion rate depending on the NO diffusion coefficient (D_{NO}) and the effective distance over which NO diffuses (d_{eff}). Some of the produced NO, on the other hand, is consumed by other reactions within the cell with a time constant (τ_{NO}) (Vaughn et al., 1998),

$$v_{NOdecay,n} = \left(\frac{1}{\tau_{NO}}\right) NO_n \tag{3.17}$$

NO concentration in smooth muscle is determined by the NO diffusion from the neuron ($v_{NO,sm}$) and the NO decay within the smooth muscle ($v_{NOdecay,sm}$). The smooth muscle volume fraction (V_{sm}) is assumed to be the same as V_c.

$$\frac{dNO_{sm}}{dt} = v_{NO,sm} - v_{NOdecay,sm} \tag{3.18}$$

The NO decay in smooth muscle is given by [104] as

$$v_{NOdecay,sm} = \left(\frac{1}{\tau_{NO}}\right) NO_{sm} \tag{3.19}$$

where NO_{sm} is the NO concentration in smooth muscle.

Using the results of a mathematical model of the nitric oxide/cGMP pathway in the vascular smooth muscle cell ([118]), NO inhibition of calcium in smooth muscle is obtained via a fit

$$Ca_{sm}^{+2} = -1785\ ln\,(NO_{sm}) + 8630 \tag{3.20}$$

3.6 Modulation of Vascular Tone

We relate the arteriolar diameter to the partial pressure of CO_2 in the precapillary arterioles using the information in [119]. Poiseuille's law states that the flow of blood through a vessel is proportional to the fourth power of the vessel diameter. Using the pCO_2 vs CBF graph in Wang et al's work, we recalculated the pCO_2 vs diameter

graph with the assumption that 40 mmHg corresponds to the normal CO_2 levels in the vessel. We then fit a curve to this new graph and the curve fit formula is given in Eq. 3.21 where d_{CO_2} represents the fractional change in diameter. It well matches with former work of Muizelaar et al. where they find a relationship directly between pCO_2 in mmHg and fractional diameter [120].

$$d_{CO_2} = 6 \times 10^{-5}\ pCO_2^2 + 0.0027\ pCO_2 - 0.2 \tag{3.21}$$

$$pCO_2 = \frac{CO_{2c}}{\alpha_{CO_2}} \tag{3.22}$$

We have related CO_2 concentration to CO_2 partial pressure (pCO_2) using the carbon dioxide solubility coefficient (α_{CO_2}). Baseline CO_2 pressure in the vessel is assumed to be 40 mmHg [101].

The fractional diameter change of the arteriole related to NO production is obtained in terms of the smooth muscle calcium concentration (Ca_{sm}^{2+}) using the data in Schuster et al's work (Figure 4A in [121]). We selectively picked the diameter and calcium values at various time instances in the above mentioned work. We then converted this data into % change of diameter and calcium by normalizing it with the maximum fluorescence intensity. Then a new graph of diameter vs Ca^{2+} was obtained to which a curve was fit to obtain Eq. 3.24.

$$d_{NO} = \frac{631000}{460600 + exp\left(12 \left\| Ca_{sm}^{+2} \right\|\right)} \tag{3.23}$$

$$\left\| Ca_{sm}^{+2} \right\| = \frac{Ca_{sm}^{+2}}{Ca_{sm,max}^{+2}} \tag{3.24}$$

where the value of $Ca_{sm,max}^{2+}$ is given in Table 3.3.

The vascular radii (in units of meters) is then calculated by simple addition of the CO_2 effect (Eq. 3.21) and the NO effect (Eq. 3.23),

$$R = 5 \times 10^{-6} \left(1 + d_{NO} + d_{CO_2}\right) \tag{3.25}$$

3.7 Model Outputs: Flow, Venous Volume, deoxy-Heamoglobin Concentration and BOLD Signal

In the model, a hypothetical brain volume is formed to include a neuron, precapillary arteriole and venous compartments that are forming a unit voxel. Assuming the total BOLD signal being a volume-weighted sum of the signals coming from individual voxels [56] and using Davis' equation [11] which links normalized $CMRO_2$ and CBF changes to the BOLD signal change, we can then calculate the percent change in BOLD signal within a voxel due to neuronal activation. Hence, the CBF, CBV and BOLD are calculated as follows:

The flow (F_{in}) in the precapillary arteriole is calculated using the Poiseuille equation with the parameters: radii (R), pressure difference across the two ends of the precapillary arteriole (ΔP), viscosity of the blood (μ) and the length of the vessel (L). We have normalized this flow with arteriole volume in order to have dimensions consistent with Aubert and Costalat's model [83].

$$F_{in} = \frac{\pi R^4 \Delta P}{8 \mu L V_{arteriole}} \tag{3.26}$$

$$V_{arteriole} = \pi R^2 L \tag{3.27}$$

The output flow from the venous compartment is obtained from the following equation [57, 122]

$$F_{out} = \frac{V_v^{\alpha'+\beta}}{V_{v,0}^{\alpha'+\beta}} F_{in,0} \tag{3.28}$$

In Eq. 3.28 we assume laminar flow ($\alpha' = 2$), and constant β represents diminished volume reserve at elevated pressures. We are using $\beta = 2$ as representative of the range of $1 \leq \beta \leq 3$ from the literature [57, 109].

The following equation [56] is used for venous volume calculations,

$$\frac{dV_v}{dt} = F_{in} - F_{out} \tag{3.29}$$

where F_{in} and F_{out} are calculated using Eqs. 3.26 and 3.28.

The deoxy-Heamoglobin (dHb) concentration and the BOLD signal are calculated by [56, 11] respectively:

$$\frac{ddHb}{dt} = 2F_{in}\left(O_{2a} - O_{2c}\right) - F_{out}\frac{dHb}{V_v} \tag{3.30}$$

$$BOLD = \frac{\Delta S}{S_0} \tag{3.31}$$

$$\frac{\Delta S}{S_0} = M\left[1 - \left(\frac{CMRO_2}{CMRO_{2,0}}\right)^{\beta'}\left(\frac{CBF}{CBF_0}\right)^{\alpha'-\beta'}\right] \tag{3.32}$$

with the parameters O_{2a}, M and β' given in Table 3.3. O_{2c} is the precapillary arteriole oxygen concentration.

3.8 Solving the Ordinary Differential Equations

The model is comprised of 20 variables. Volumes, areas and cerebral blood flow values are all expressed per unit tissue volume. In order to solve the ordinary differential equations, we have used the ode23s tool of MATLAB7.5 for stiff equations. Besides the equations given in sections above, the first 13 equations in Table 1 in Aubert and Costalat's model [83] are used in this model with the corresponding parameters within the same work.

3.9 Assumptions

We set CBF dependent solely on radii changes with the assumption that the local CBF changes in precapillary arterioles are dependent more on diameter changes of the vessels than the pressure difference between the two ends of them, which may not be the case during systemic changes (heart rate, stroke volume etc.) activated during brain function.

We have also assumed that the NO and CO_2 effect on blood flow are independent of each other. Although previous research on rats suggest that inhibition of nitric oxide synthase reduces the CBF response to hypercapnia [80], more recent research on humans found no significant change in CBF response to hypercapnia under NOS inhibitors [81]. We base our model on this more recent finding.

The fourth assumption to be mentioned here is that the energy consumption during brain activation is solely due to the Na^+-K^+ pump. Actually when the Na^+-K^+-ATPase is blocked in the whole brain, the energy usage drops dramatically [6], a fact which makes this assumption acceptable.

We modeled the action of NO and Ca^{2+} on pre-capillary arterioles since they have smooth muscle cells which dilate actively by using NO and Ca^{2+} signaling pathways.

We have also assumed that Ca^{2+} entry into channels is solely through NMDA channels. Our assumption is based on the studies which show that calcium elevation due to synaptic activity is almost totally blocked in the presence of NMDA channel blocker AP5 [123, 124, 125].

Table 3.2
Parameters for the rate equations.

Eqn	Constant	Description	Reference
1	$a_1 = 34.83$	Fitting constants	
	$b_1 = 0.0001904$	for a single action potential	
	$c_1 = 0.001559$		
	$a_2 = 37.97$		
	$b_2 = 0.002051$		
	$c_2 = 0.0002703$		
	$a_3 = 40.96$		
	$b_3 = 0.002259$		
	$c_3 = 0.0001748$		
	$a_4 = 75.48$		
	$b_4 = 0.001903$		
	$c_4 = 0.0005914$		
	$a_5 = -597 \times 10^{15}$		
	$b_5 = -0.7747$		
	$c_5 = 0.1367$		
4	n_{Aero}=3	Stoichiometric constant	[83]
5a,b	D_{new,CO_2}=1.31 s^{-1}	Diffusion rate for CO_2	See text for calculation.
5b	D_{CO_2}=1.61×$10^{-5}$$cm^2/s$	Diffusion Constant for CO_2	[100]
5b	d_{eff}=35	Effective diffusion distance for CO_2	The same value as for NO. (see below)
7	$CO_{2a} = 0.635$ mM	CO_2 concentration in arteriole	[101]
9	$\tau_{Ca^{2+}}$=0.780 s	Decay Constant for Calcium	[102]

Table 3.3
Parameters for the rate equations.

Eqn	Constant	Description	Reference
12a,b	$D_{new,NO}$=1.31 s^{-1}	Diffusion rate for NO	See text for calculation.
12b	D_{NO}=4×$10^{-5}$$cm^2$/s	Diffusion constant for NO	[78]
			[103]
12b	d_{eff}=35	Effective diffusion distance for NO	[104]
13,15	τ_{NO} = 0.5 s	Decay Constant for NO	[104]
17b	α_{CO_2}=0.0308	Solubility Constant for CO_2	[101]
	$mmolL^{-1}mmHg^{-1}$		
18b	$Ca^{+2}_{sm,max}$ = 3563 nM	Maximum Ca^{2+} concentration	[105]
		in smooth muscle	
20a	ΔP=266.6 kg/ms^2	Pressure difference	[106]
		between the two ends of	
		a precapillary arteriole	
20a	μ=0.001 kg/ms (0 % Hct)	Viscosity	[107]
	μ=0.01 kg/ms (45 % Hct)		
20b	L=1.8 mm	Length	[108]
		of a precapillary arteriole	
21	$\alpha' = 2$	Laminar flow	[57]
21	$\beta = 2$	Vascular compliance parameter	[109]
21	$V_{v,0}$ =0.0237	Initial venous volume fraction	[56]
21	F_{in} =0.0217 s^{-1}	Initial flow in	[56]
23	O_{2a} =8.34 mM	Total arterial oxygen concentration	[110]
24b	M =0.25	M value	[111]
24b	$\beta' = 1.5$	Imaging parameter	[11]

4. METHODS - EXPERIMENT

In vivo imaging experiments were performed using Sprague Dawley rats undergoing 4, 10 and 20 s long electrical forepaw stimulation.

4.1 Animal Preparation

Male Sprague Dawley rats (n=12; 250-350 g) were used for the study. Animal protocols were approved by the Massachusetts General Hospital Subcommittee on Research Animal Care. Rats were anesthetized with isofluorane, 3% initially and 2% (in 25% oxygen, 75% air) during ventilation while surgery was being performed. The tracheotomy, femoral arterial and venous catheters were placed before the surgery.

Tracheotomy: Rats were placed prone, and ventral neck area was shaved. A midline incision was opened and subcutaneous tissue and the pre-tracheal muscle layers were dissected away under retraction. A horizontal incision was placed between the first and second tracheal rings and an endotracheal cannula was inserted and tied in place. After ensuring a patent airway, the subcutaneous tissue and skin was sutured using 4-0 silk. Endotracheal catheter was connected to a small animal respirator.

Arterial/venous catheterization: The left femoral area was shaved. The femoral artery was isolated after skin incision (1.5 cm in length) and dissection of the soft tissue. Two sutures were passed under the femoral artery and proximal portion was clamped. A small incision was made on the arterial wall and a PE-50 polyethylene catheter was inserted and tied in place. Good arterial pulsations were confirmed by removing the clamp. The same cannulation procedure was done to femoral vein. Catheters were flushed with sterile heparinized saline containing 2 Units heparin/cc. The subcutaneous tissue and skin were sutured using 4-0 silk.

The head of the animal was fixed in a stereotaxic frame using ear bars. For the spectroscopic imaging experiments, the scalp was retracted and the area of skull overlying the primary somatosensory cortex was thinned. Cerebrospinal fluid was drained from the IVth ventricle to relieve intracranial pressure. For the two photon microscopy experiments, the thinned skull and dura matter were removed. The anesthesia was switched from isofluorane to alpha-chloralose. Alpha-chloralose was maintained with 50 mg/kg intravenous bolus of alpha-chloralose followed by continuous intravenous infusion at 40 mg $kg^{-1}h^{-1}$. Heart rate, blood pressure, and body temperature were continuously monitored. The animal's blood measurements were aimed to be maintained as this: pCO_2 between 35 and 45 mmHg, pO_2 between 140 and 180 mmHg, and pH between 7.35 and 7.45. The body temperature of the animal was maintained at 37.0 $\pm$ 0.5°C with a homeothermic blanket (Harvard Apparatus, Holliston, MA, U.S.A.) during surgery and experiments. Blood samples ($\cong$0.05 ml) were withdrawn from the anesthetized rat for blood gas measurement (not exceeding 5 total; $\cong$0.25 ml).

4.2 The Stimulus

For the spectroscopic optical imaging, the stimulus consists of a train of three electrical pulses (3 Hz repetition rate, 300-μs-wide, 0.5-1.5 mA pulse amplitude, 4 s pulse train duration, 20 s stimulation sequence period) delivered to a forepaw through a pair of thin needles implanted under the skin which were connected to an electrical stimulus isolation unit (WPI Inc, Sarasota, FL, USA). The intensity of the stimulus was adjusted to provide stimulation below the movement threshold. For the two-photon microscopy, the same stimulus was applied for 4, 10 and 20 s train duration with the stimulation sequence periods of 30, 40 and 50 s.

4.3 Optical Imaging

Spectroscopic optical imaging We have determined the active brain region during forepaw stimulation using optical intrinsic signal imaging (OISI). For OISI, an Hg:Xe lamp illumination was spectrally filtered to a narrow band at 570 nm which is the isosbestic point for hemoglobin absorption. At this wavelength, any decrease in cortical reflectivity likely corresponds to an increase in total hemoglobin. Images from the thinned-skull were acquired by cooled 12-bit CCD camera (Imager QE, La Vision). The spectral data were converted to percent-change maps for total hemoglobin (HbT) using the modified Beer-Lambert law.

Two-Photon Microscopy. A chamber consisting of a metal frame (Kleinfeld and Delaney) and a removable glass cover slip (number 1) lid was glued to the skull. The cover slip reduces brain motion and protects it from contamination and dehydration. The space between the brain surface and the cover glass was filled with 0.7% (w/v) agarose (Sigma) in artificial cerebrospinal fluid. An amount of 0.3 ml of 5% (w/v) solution of 2 MDa fluorescein isothiocyanate conjugated dextran (FD-2000S; Sigma), which is a dye labeling blood plasma, was injected intravenously to enhance the visibility of the blood vessels. Images were obtained using 4-channel Ultima two-photon laser-scanning microscope (Prairie Technologies). The open brain region was diffusely illuminated with a laser tuned to 740 nm. Before the actual experiment, we obtained an image of the entire cranial window using a 4X air objective (XLFluor4X/340; numerical aperture (NA), 0.28; Olympus, Tokyo, Japan) to aid in navigating around the cortical vasculature. The line scan measurements which require high resolution were obtained using 10X (NA, 0.3; Olympus) air-spacing and 20X (NA, 0.95; Olympus, working distance: 2 mm) water-immersion objectives. Line scans were acquired with a scan rate of 1.3 kHz and a scan resolution of 0.6 μm (for an example please see Figure 4.1. The data was acquired until the response amplitude start to decrease, indicating a general deterioration of physiological conditions. Data analysis was performed in MATLAB (MathWorks, Inc.).

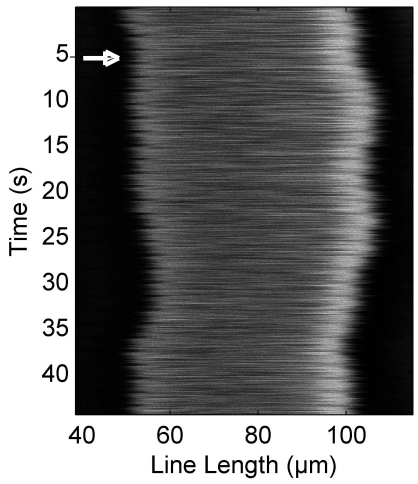

Figure 4.1 Image constructed by the addition of line scans across a vessel during forepaw stimuli.

4.4 Calculations of the Parameters

We recorded the first 5 seconds before stimulation to calculate baseline diameter. The amplitude of the peak response (μm) is calculated by subtracting the baseline diameter from maximum dilation. Figure 4.2 shows the characteristics calculated in the work. The fraction of the peak response (%) is the percent dilation with respect to baseline diameter. Time to peak (s) is the time difference between the time the dilation peaks and the stimulus onsets. The width of the maximum (s) is the full width at 25 % of the peak response. The amplitude of the post-stimulus undershoot (μm) is calculated by subtracting the maximum constriction after the stimulus from baseline diameter. The fraction of the post-stimulus undershoot (%) is the percent constriction with respect to baseline diameter. The falling time (s) is the difference between the time at which dilation falls to the half of the maximum dilation and the end of stimulus duration. The width of the minimum (s) is the full width at 30 % of the peak constriction after the stimulus.

Statistical Analysis: We have classified the groups according to two independent variables: caliber size (smaller diameter group $<$40 μm and larger diameter group $>$40 μm) and stimulus duration (4, 10 and 20 second stimulus durations) forming a total of 6 groups. We used one-way Analysis of Variance (ANOVA) to test whether the measured

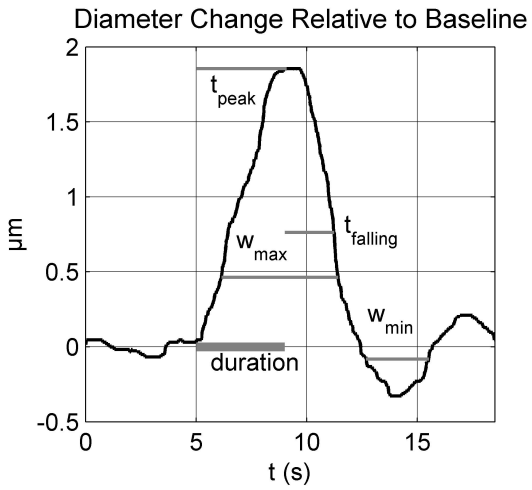

Figure 4.2 Transient dilation characteristics.

characteristics of the same caliber-size groups are actually different at different stimulus durations, and also to test whether these measured values at the same stimulus duration are actually different at different caliber sizes.

5. RESULTS - MODELING

We plot Ca^{2+} and Na^{+} dynamics in the neuron as a response to a stimulus lasting 20 seconds and 100 seconds (Figure 5.1). A sample part from the stimulus in Figure 5.1A, shows the change in membrane voltage, i.e. action potentials, during the stimuli.

To explore the relative roles of the vasoactive agents NO and CO_2 in the stimulus evoked change in CBF, in Figure 5.2 we plot the relative change in CBF (rCBF) for a short (20 second) and long (100 second) duration stimulus considering modulation of the vascular tone by NO only, CO_2 only, and both NO and CO_2.

The largest change in CBF is observed with NO only, while CO_2 alone is producing only a small increase in CBF. When both NO and CO_2 effects on vascular tone are considered, the CBF response is reduced relative to NO alone. We observe a flow overshoot during the first 10 seconds of the stimulus, a significant post-stimulus undershoot for the short stimulus, and a slow post-stimulus recovery for the long-stimulus. These results reveal that the vessels may dilate or constrict depending on the balance of CO_2 production by the mitochondria and washout by the flowing blood.

In Figure 5.3 we plot the evoked changes in the BOLD signal corresponding to the differing flow responses from NO only, CO_2 only, and both NO and CO_2 modification of vascular tone. Inhibiting the effect of NO significantly reduces the flow response (see Figure 5.2) leading to a negative BOLD response as the reduced flow response does not oversupply the increased demand for oxygen. Considering the effects of both NO and CO_2 compared with NO alone attenuates the peak BOLD response during the stimulus and modifies the post-stimulus BOLD undershoot, increasing the undershoot for a short stimulus and diminishing its duration for long stimulus. This modification of the post-stimulus BOLD undershoot is due to a slow $CMRO_2$ recovery and the post-stimulus flow undershoot.

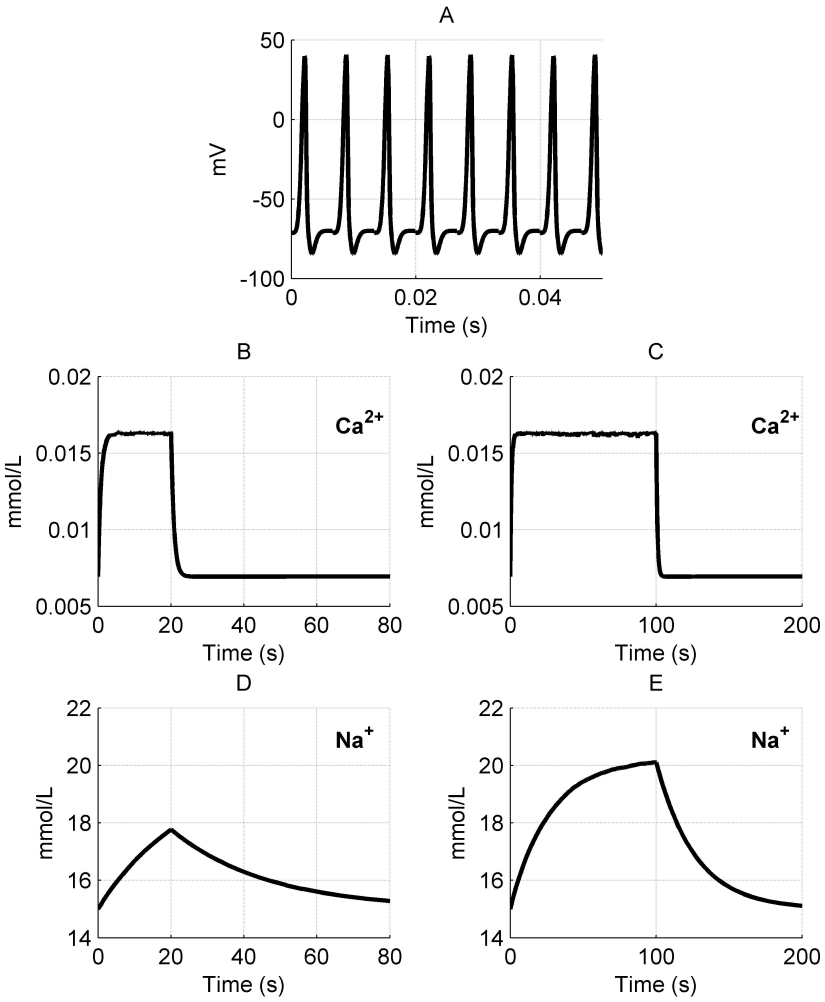

Figure 5.1 The input function of the model: a series of action potentials at 150 Hz (A), only a portion is shown as an example. The Ca^{2+} and Na^{+} concentration as a response to the stimulus. Results are given (B) and (D) for a 20 second stimulus and (C) and (E) for a 100 second stimulus.

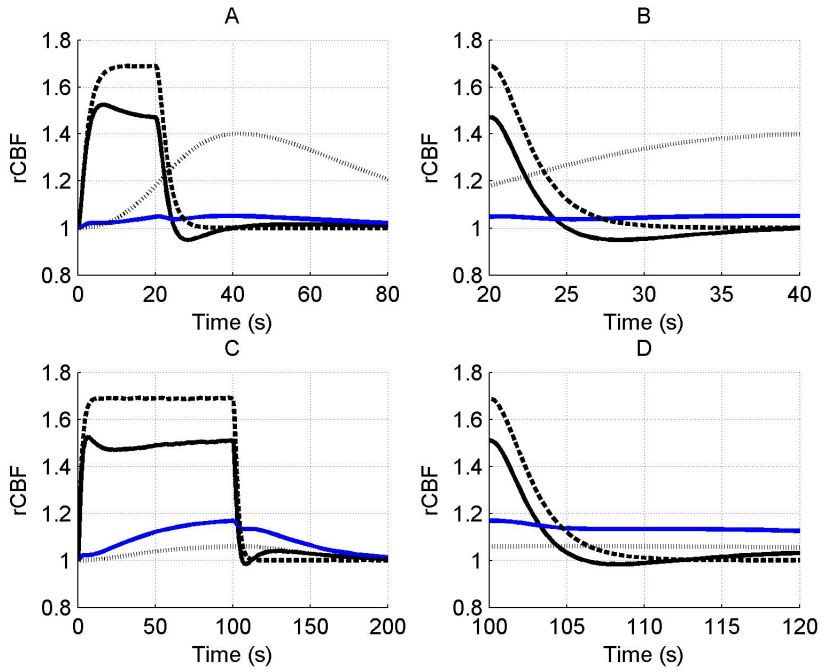

Figure 5.2 Our model results for an evoked change in CBF considering the vasoactive role of only NO (dotted black line), only CO_2 (dotted line), both NO and CO_2 (solid line). The relative change in $CMRO_2$ is indicated by the grey line. Results are given (A) and (B) for a 20 second stimulus and (C) and (D) for a 100 second stimulus. In each case we considered the stimulus as a train of action potentials at a repetition frequency of 150 Hz as input to our model. Note that in panel (A) we increased the scale of the only CO_2 effect (dotted line) by x20. CBF: cerebral blood flow, $CMRO_2$: cerebral metabolic rate of oxygen.

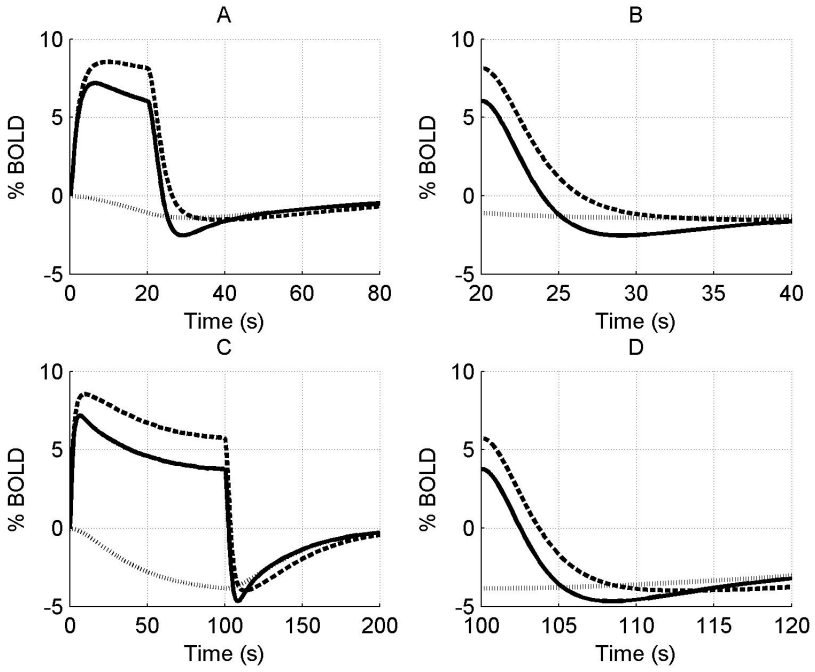

Figure 5.3 Our model results for an evoked change in BOLD signal considering the vasoactive role of only NO (dashed line), only CO_2 (dotted line), and both NO and CO_2 (solid line). Results are given (A) and (B) for a 20 second stimulus and (C) and (D) for a 100 second stimulus. In each case we considered the stimulus as a train of action potentials at a repetition frequency of 150 Hz as input to our model. BOLD: blood oxygenation level-dependent.

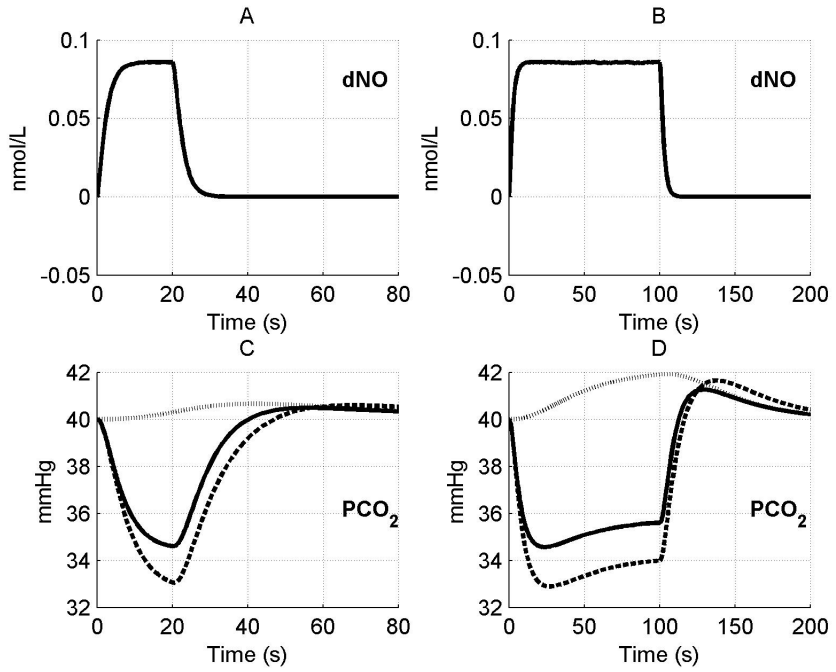

Figure 5.4 Change in NO levels in smooth muscle and the partial pressure of CO_2 in the precapillary arteriole are plotted considering the flow response from NO alone (dashed line), CO_2 alone (dotted line), and both NO and CO_2 (solid line) for the (A) 20 second stimulus and the (B) 100 second stimulus. pCO_2: partial pressure of CO_2.

The precapillary arteriole partial pressure of CO_2 pressure corresponding to the three different vasoactive effects is plotted in Figure 5.4. It is evident that the large flow response produced by NO is washing out more CO_2 than is being produced by the increased oxygen consumption, causing a reduction in the partial pressure of CO_2 akin to the washout of deoxygenated hemoglobin during a stimulus. When the effect of NO on vascular tone is neglected, we observe that the partial pressure of CO_2 increases because the flow response is too small to wash out the extra CO_2 produced by the increased oxygen consumption, consistent with the negative BOLD signal in Figure 5.3. We also observe a post-stimulus overshoot in the partial pressure of CO_2 arising from the slow recovery of oxygen consumption.

To provide support for the magnitude of the CO_2 effect in varying vascular tone in our model, we simulated the change in flow and BOLD as the systemic partial pressure of CO_2 was increased, and compared our simulation results with experimental results. The simulated results are shown in Figure 5.5 compared with experimental

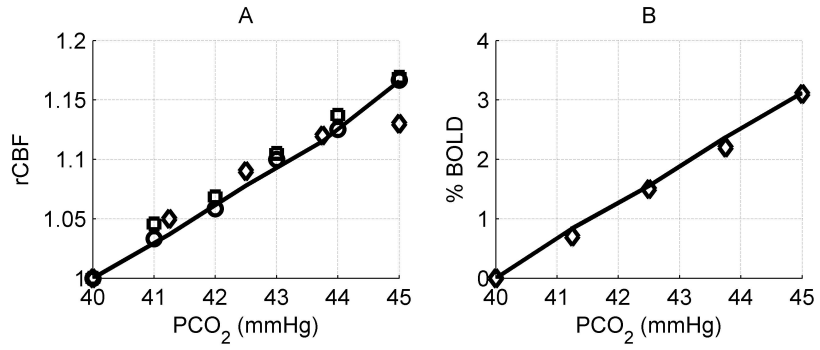

Figure 5.5 Modeled (A) CBF and (B) BOLD versus the partial pressure of CO_2 compared with experimental data from [1] circles, [2] squares, and [3] diamonds. Our model results are indicated by the solid line. CBF: cerebral blood flow, BOLD: blood oxygenation level-dependent.

data from [1, 2, 3]. Our model results well match with the experimentally observed flow changes and the BOLD changes.

We have performed a sensitivity analysis to verify the robustness of the CBF post-stimulus behavior shown in Figure 5.2. The decay constants for Ca^{2+} and NO were varied over their physiological range ($\tau_{Ca^{2+}}$: 0.5-1 s [126], τ_{NO}: 0.5-5 s [104]). While there was a dramatic decrease in the CBF undershoot as we increased $\tau_{Ca^{2+}}$, we none-the-less still observe an undershoot at $\tau_{Ca^{2+}} = 1$ s. We observed that NO had no significant effect on the CBF undershoot. In addition, the diffusion constants for NO (3.3×10^{-5} - 4.8×10^{-5} cm^2/s, [103, 78]) and CO_2 (1.14×10^{-5} to 2.5×10^{-5} cm^2/s, [127]) have a negligible effect on the undershoot results. Increasing the maximum Na conductance (g_{Na}) decreases the undershoot, completely abolishing it when $g_{Na} > 15$ mS/cm^2 (we used 4.4 mS/cm^2 [128]). Varying NMDA conductance (g_{NMDA}) had no effect on the undershoot over the range of 500 to 1350 μM/(msec.mV) [114].

6. DISCUSSION - MODELING

The results of our model confirm the expected dominant vasodilatory role of NO, however CO_2 is also important in modulating the shape of the response, in particular the initial overshoot and post-stimulus undershoot. Our results indicate that a washout of CO_2 has a vasoconstrictive effect throughout the stimulus because NO dominates the blood flow response. While the vasoactive role of NO in producing a blood flow response is known experimentally [129, 130, 69], there is no experimental support for the possible blood flow effects of locally-produced-CO_2.

The transient increase in nitric oxide, as reported in the literature, varies widely. While there are some studies showing the change to be as low as 2.2 nM in rats after parallel fiber stimulation [131] and 0.3 nM in cat nucleus tractus solitarius after arginine application [132], some values are as high as 80 nM in cat after visual stimulus [63] and 200 nM in rats after forepaw stimulus [64]. We also varied the decay constants for NO over their physiological range τ_{NO}: 0.5-5 s [104]. Our sensitivity analysis showed that NO had no significant effect on the CBF undershoot. The shape of the reported NO responses also varies as stimulus type changes. The shape of the NO change in our model is more similar to the experimentally measured response for a visual stimulus [63], than for a forepaw stimulus [64].

A post-stimulus CBF undershoot has been observed by numerous groups. Specifically, the CBF undershoot has been observed in rat somatosensory cortex [133, 134], cat visual cortex [135], and human visual cortex [136, 137, 38, 138, 139]. Our simulations also result in a post-stimulus CBF undershoot. Our results show that the interplay between NO and CO_2 is a possible explanation for this undershoot, without ruling out the effect of other possible confounding mechanisms such as neuronal inhibition.

The positive BOLD response is determined by the relative contributions of CBV, CBF and $CMRO_2$. When the effect of only NO and both NO and CO_2 are considered, a positive BOLD response is obtained during the stimulus. Inhibiting the effect of NO diminishes the CBF increase significantly and so results in a negative BOLD response due to the insufficient oxygen supply to the activation area. This result is supported by various experimental efforts to determine the effect of NO in neurovascular coupling. Stevanovic et al. showed that inhibiting nitric oxide synthase significantly attenuates the CBV, CBF and BOLD responses [68]. Since this inhibition of nitric oxide is not one hundred percent, and it also diminishes the neural activation though less strongly, they still obtained a very low but still positive BOLD response. Findings from other works also suggest that the positive BOLD response is abolished by the inhibition of nitric oxide [140].

For the post-stimulus BOLD undershoot, three mechanisms have been suggested: 1) sustained oxygen consumption after CBF has returned to baseline [141, 142], 2) a slow recovery of CBV to baseline compared to CBF

In summary, the increase in CBF during stimulation likely reduces local tissue pCO_2. This is another possible explanation for the post-stimulus CBF undershoot that has been described in the literature. It should also be added that the relative contributions of these different mechanisms of vasoregulation will likely be altered in cerebrovascular diseases.

7. RESULTS - EXPERIMENT

We have examined the effect of baseline vessel diameter and stimulus duration on the hemodynamic response during somatosensory stimulus as well as during the post-stimulus period following it. The typical response was that the vessels first dilated to a peak amplitude, and then recovered to a lower dilation and kept this dilated form until the end of stimulus duration (Figure 7.1). We analyzed the dilation transients so that we could extract more information about the hemodynamic response, in particular, dependence of temporal characteristics of response on stimulus duration and baseline diameter or in other terms proximity to the activation area, since the feeding pial vessels are larger compared to perforating diving vessels which are located closer to the activation area. The latter was aimed to give insight to retrograde dilation hypothesis.

The hemodynamic measures we investigated are: the amplitude and the percentage of the peak response, time to peak response, the width of the maximum response, and the amplitude and percentage of the post-stimulus undershoot, falling time to minimum of the undershoot and width of the undershoot among different baseline diameter groups (caliber sizes with 10 μm increments) with the help of ANOVA test (for a detailed description of the parameters, please see Methods section). As the overall results for the peak response percentage (Figure 7.2), time to peak (Figure 7.3) and post-stimulus undershoot percentage (Figure 7.4) show a clear grouping of the diameters, the data is further analyzed in two groups, namely diameters smaller and larger than 40 μm. Also, the two groups are analyzed for different stimulus durations.

7.1 Peak Response Amplitude Changes with Caliber Size but not with Stimulus Duration.

The peak response amplitude is further analyzed for the two caliber groups in Figure 7.5, the p values are given for the ANOVA test results across the two caliber

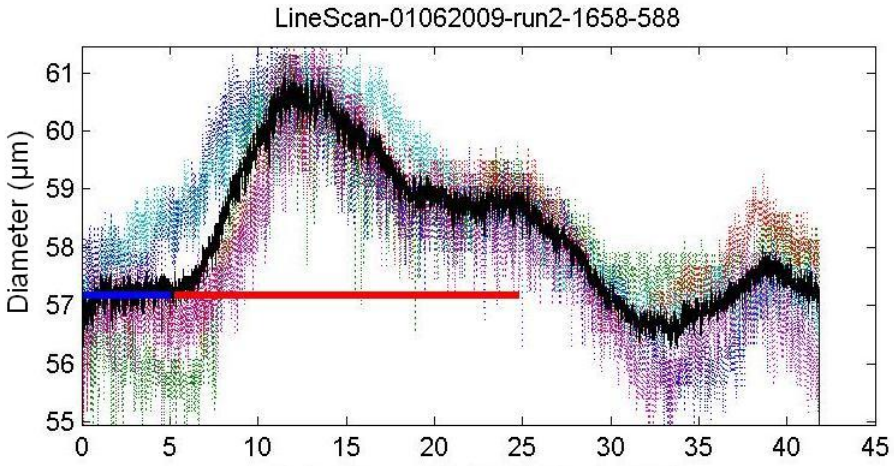

Figure 7.1 Time course of the dilation of an arteriole during a 20 second stimulus (grey line: stimulus duration, black line: averaged response of five individual trials).

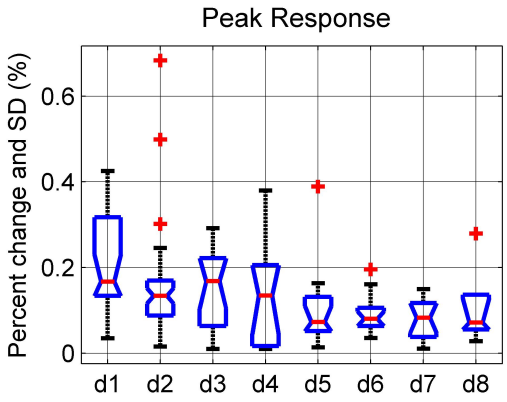

Figure 7.2 Peak response percentage at 10 µm increments of diameter with a p value of 0.02 from ANOVA test. (All stimulus durations are included.)

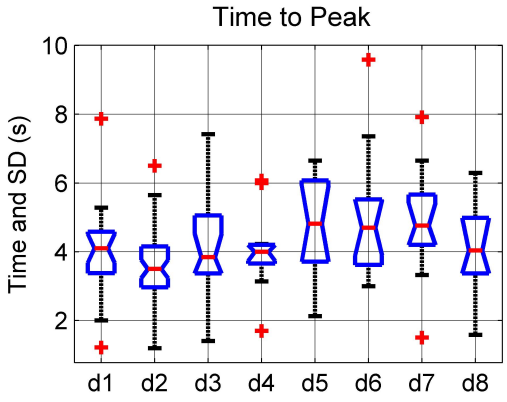

Figure 7.3 Time to peak at 10 µm increments of diameter with a p value of 0.008 from ANOVA test. (All stimulus durations are included.)

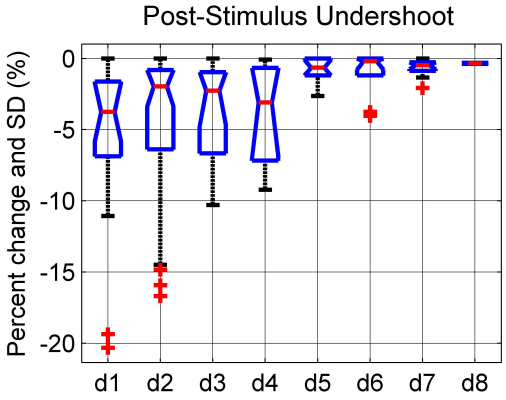

Figure 7.4 Post-stimulus undershoot percentage at 10 µm increments of diameter with a p value of 0.004 from ANOVA test. (All stimulus durations are included.)

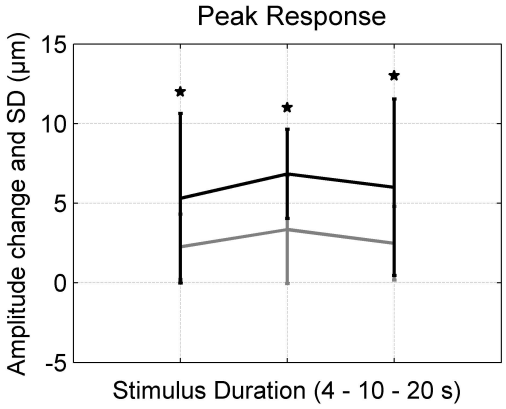

Figure 7.5 Peak response for 4, 10 and 20 second stimulus durations (grey $<$ 40 µm, black $>$ 40 µm).

groups and across the three stimulus durations in Table 7.1. The peak response amplitude is significantly higher for the larger vessel group (Figure 7.5). Our result is in conformity with the previous studies. Segal et al who investigated the dilation of arteries and arterioles of hamster skeletal muscle also found that arteries dilate amplitude-wise more compared to arterioles [143]. On the contrary no significant difference in peak response amplitude is found between stimulus durations (Figure 7.5). A study by Ngai et al. also shows that increasing stimulus duration has no effect on the peak response amplitude of the pial arteriole in sensory hindlimb cortex to sciatic nerve stimulation [144].

Table 7.1
Peak response amplitude (mean and standard deviation)

Diameter	4	10	20	p
<40 μm	2.26 (±2.05)	3.35 (±3.39)	2.48 (±2.31)	0.27
>40 μm	5.31 (±5.33)	6.84 (±2.8)	6.0 (±5.54)	0.79
p	0.005*	0.02*	0.009*	

7.2 Peak Response Percentage Changes with Caliber Size but not with Stimulus Duration.

Our results for peak response percentage for each caliber size group during 4, 10 and 20 s stimulus durations are shown in Figure 7.6. While the mean peak response percentage for each stimulus duration is higher for the smaller diameter group, the variance is significant only for the 4 second stimulus and marginally significant for the 10 second stimulus (Figure 7.6 and Table 7.2). Our results are in accordance with the work of Iadecola et al. in which they showed with the use of a videomicroscopy system that the smaller vessels are more reactive than larger ones during rat cerebellar parallel fiber stimulation [93]. Their work comprises a vessel diameter range of 10-40 μm which corresponds to our smaller diameter group. The percent-wise peak response increase they obtained in this diameter range is totally consistent with our results. The same result is also obtained by correlating baseline artery size to flow mediated dilation [145]. On the other hand, we found no significant difference in peak response percentage between three stimulus durations.

Table 7.2
Peak response percent change (mean and standard deviation)

Diameter	4	10	20	p
<40 μm	15 (±13)	18 (±11)	15 (±9)	0.54
>40 μm	9 (±7)	11 (±5)	10 (±10)	0.71
p	0.04*	0.11	0.15	

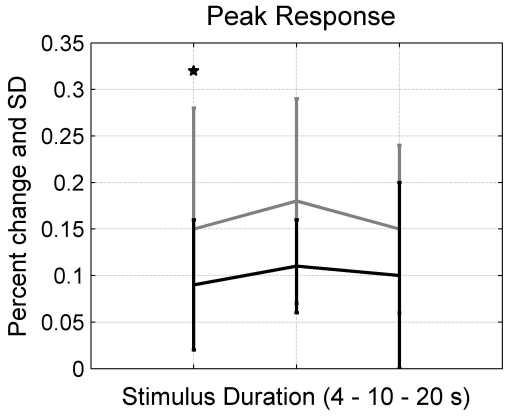

Figure 7.6 Peak response percent change for 4, 10 and 20 second stimulus durations (grey $<$ 40 μm, black $>$ 40 μm).

7.3 Time to Peak Values: Smaller vessels Dilate First.

Time to peak values for each group at three stimulus durations is given in Figure 7.7 with the corresponding p values in Table 7.3. The time to peak values obtained in our work are amplitude-wise consistent with the previous measurements of dilation by Ngai et al. using a video micrometer [144]. Our results show that larger vessels have around 1 second delay in average in responding the stimulus with respect to smaller vessels, a finding supporting the retrograde dilation. A recent work from Chen et al found that superficial cortical regions have around a 2 second delay response compared to the deeper regions using Optical Coherence Tomography (OCT) [9]. Time to peak values is shorter for 4 second stimulus compared to 10 and 20 second durations; on the other hand it is almost constant for the stimulus durations longer than 4 second, consistent with the previous observations by Ngai et al. [144].

Table 7.3
Time to peak in seconds (mean and standard deviation)

Diameter	4	10	20	p
$<$40 μm	3.52 (±1.22)	3.89 (±1.17)	4.09 (±1.26)	0.13
$>$40 μm	3.97 (±1.43)	5.08 (±1.36)	5.26 (±1.36)	0.03*
p	0.22	0.04*	0.01*	

To test whether this difference is due to the different vessel properties or due

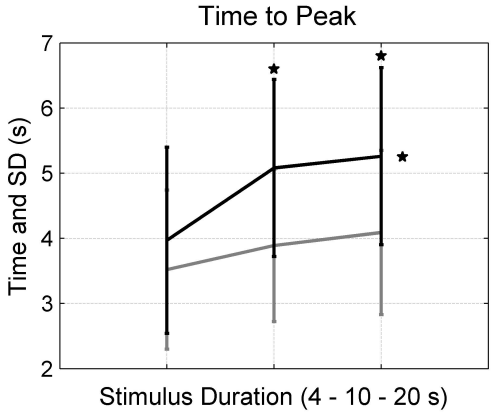

Figure 7.7 Time to peak for 4, 10 and 20 second stimulus durations (grey $<$ 40 μm, black $>$ 40 μm).

to a delay in upstream large vessels, we further analyzed the data at stimulus onset. We averaged the time to peak differences of the smaller and larger diameter groups for the 10 and 20 second stimulus durations where it reaches almost a constant value (for 10 s stimulus (1.17 s) and for the 20 s (1.19 s) stimulus). We obtained the percent diameter increase at this time period of stimulus onset. The small diameter group's increase is around 1.5 %, while larger diameter group's increase is only 0.5 %. We have also found out that at almost 0.8 from stimulus onset, vessels larger than 50 μm do not start dilating at all, a finding strongly supporting the retrograde dilation hypothesis.

7.4 Width of the Maximum Changes with Stimulus Duration but not with Caliber Size.

The width of the dilation of smaller and larger vessel groups at three different stimulus durations are shown in Figure 7.8. There is no significant difference between the smaller and larger diameter groups in terms of the width of the dilation. However, there is a significant difference among different stimulus durations, width being longer for longer stimulus durations. Our results are in good agreement with previous findings from Ngai et al. [144].

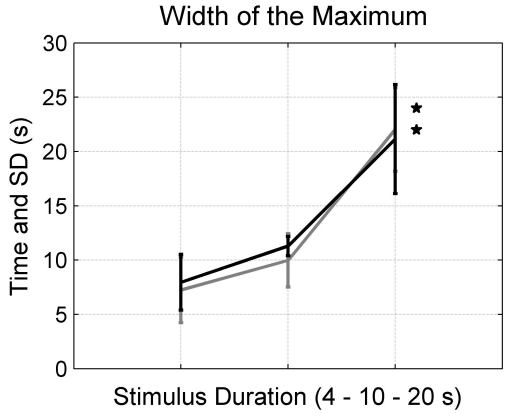

Figure 7.8 Width of the maximum for 4, 10 and 20 second stimulus durations (grey $<$ 40 µm, black $>$ 40 µm).

Table 7.4
Width of the maximum in seconds (mean and standard deviation)

Diameter	4	10	20	p
<40 µm	7.25 (±3.02)	9.97 (±2.45)	22.03 (±3.87)	<0.001*
>40 µm	7.95 (±2.57)	11.29 (±0.88)	21.14 (±5.02)	<0.001*
p	0.45	0.18	0.29	

7.5 Post-Stimulus Undershoot Amplitude is Higher for Smaller Diameter Group.

The post-stimulus undershoot amplitudes for smaller and larger groups at three different stimulus durations are shown in Figure 7.9 with the corresponding ANOVA results in Table 7.5. We observed no significant difference with caliber size or with stimulus duration. However, the mean post-stimulus undershoot amplitude for each stimulus duration is higher for smaller diameter group.

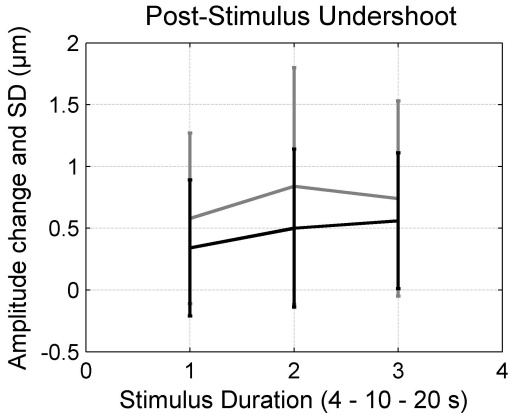

Figure 7.9 Post-Stimulus undershoot amplitude for 4, 10 and 20 second stimulus durations (grey $<$ 40 μm, black $>$ 40 μm).

Table 7.5
Post-stimulus undershoot amplitude (mean and standard deviation)

Diameter	4	10	20	p
$<$40 μm	0.58 (±0.69)	0.84 (±0.96)	0.74 (±0.79)	0.48
$>$40 μm	0.34 (±0.55)	0.50 (±0.64)	0.56 (±0.55)	0.61
p	0.26	0.43	0.5	

7.6 Post-stimulus Undershoot Percentage Changes with Caliber Size but not with Stimulus Duration.

The post-stimulus undershoot percentage for smaller and larger groups at three different stimulus durations are shown in Figure 7.10 with p values in Table 7.6. The smaller diameter group has significantly higher post-stimulus undershoot percentage. On the other hand, no significant difference is observed with changing stimulus duration. Chen et al calculated CBV undershoots from the CBV measurements when the BOLD post-stimulus undershoot occurs. They observed no significant difference in CBV post-stimulus behaviors between two stimulus durations: 24 and 96 s [139].

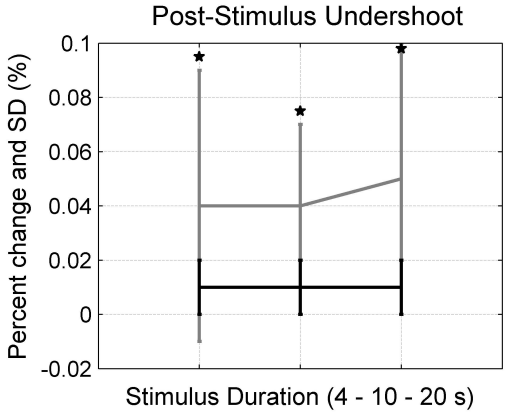

Figure 7.10 Post-stimulus undershoot percentage for 4, 10 and 20 second stimulus durations (grey $<$ 40 μm, black $>$ 40 μm).

Table 7.6
Post-stimulus undershoot percentage (mean and standard deviation)

Diameter	4	10	20	p
$<$40 μm	4 (±5)	4 (±3)	5 (±5)	0.92
$>$40 μm	1 (±1)	1 (±1)	1 (±1)	0.65
p	0.02*	0.02*	0.03*	

7.7 The Falling Time Decreases with Increasing Stimulus Duration.

The falling time is significantly longer for the larger diameter group for 4 s stimulus and the variance is not significant for the 10 and 20 second stimulus durations (Figure 7.11 and Table 7.7). On the other hand, the falling time decreases significantly at longer stimulus durations. Note that a negative falling time indicates that dilation falls down to its half before the stimulus ends.

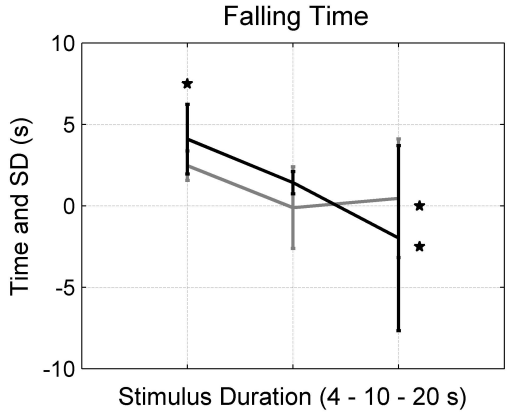

Figure 7.11 Falling time for 4, 10 and 20 second stimulus durations (grey $<$ 40 µm, black $>$ 40 µm).

7.8 Width of the Post-Stimulus Undershoot Increases with Increasing Stimulus Duration.

We also tested whether the width of the undershoot varies with baseline diameter or stimulus duration (Figure 7.12). The mean of the width of the undershoot is longer for smaller diameter vessels (Table 7.8). The width of the undershoot increases with increasing stimulus duration. The difference is significant for both groups.

Table 7.7
Falling time in seconds (mean and standard deviation)

Diameter	4	10	20	p
$<$40 µm	2.46 (±0.90)	-0.12 (±2.51)	0.46 (±3.65)	$<$0.001*
$>$40 µm	4.09 (±2.14)	1.42 (±0.68)	-1.99 (±5.68)	0.001*
p	$<$0.001*	0.16	0.09	

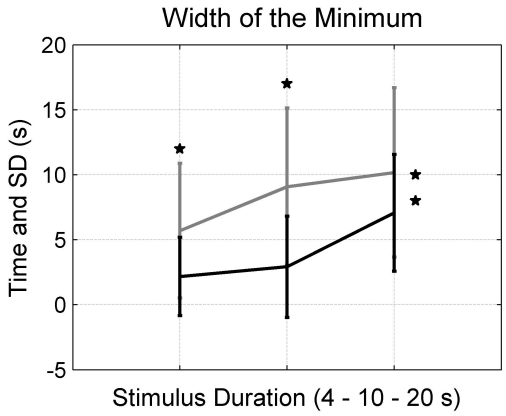

Figure 7.12 Width of the minimum for 4, 10 and 20 second stimulus durations (grey $<$ 40 µm, black $>$ 40 µm).

Table 7.8
Width of the minimum in seconds (mean and standard deviation)

Diameter	4	10	20	p
<40 µm	5.70 (±5.18)	9.08 (±6.06)	10.18 (±6.52)	0.008*
>40 µm	2.17 (±3.01)	2.92 (±3.90)	7.07 (±4.50)	0.009*
p	0.02*	0.02*	0.22	

8. COMPARISON OF THE MODELING AND EXPERIMENT

We compared our results from modeling and animal experiments related to the transient characteristics of the hemodynamic response during and after the stimulus. Our model results well match with the larger diameter group for all parameters except the width of the minimum which matches well with the smaller diameter group. In Figure 8.1, the results for peak response, time to peak and width for the response during stimulus is given. The model results show a great concordance with the experimental results. In Figure 8.2, the characteristics related to the post-stimulus undershoot are given. The percent undershoot is in a good agreement with the experimental results. While the model curve for falling time first follows the experimental well; towards 20 s stimulus the model overestimates the falling time. The model result for the width of the minimum slightly overestimates the experimentally measured widths. Note that the width of the minimum here is for the smaller vessel as mentioned above, the models overestimation increases for the larger vessel group, though the increasing behavior for an increase in stimulus duration is the same for both groups. To investigate whether the $CMRO_2$ onset and recovery kinetics during functional activity is slow (in minutes) as in PET literature or fast (in seconds) as in fMRI and optical imaging literature, we further forced the model to have a faster $CMRO_2$ increase following stimulus onset, and recovery post-stimulus with the help of a function increasing to its maximum value (10 %) in five seconds and returning to baseline after the stimulus again in five seconds representing $CMRO_2$. We compared these results obtained with this fast $CMRO_2$ kinetics, with out previous model results with slow $CMRO_2$ kinetics. We had no or little change for most of the transient characteristics (not shown). In Figure 8.3A, the minimum of the post-stimulus undershoot in diameter is given as a function of stimulus duration. Our modeling results based on slow $CMRO_2$ kinetics showed first an increase, then a peak around 10 second stimulus duration, and then a decrease in post-stimulus diameter undershoot. Our experimental results, on the other hand, show no dependency of post-stimulus diameter undershoot on stimulus duration. The result

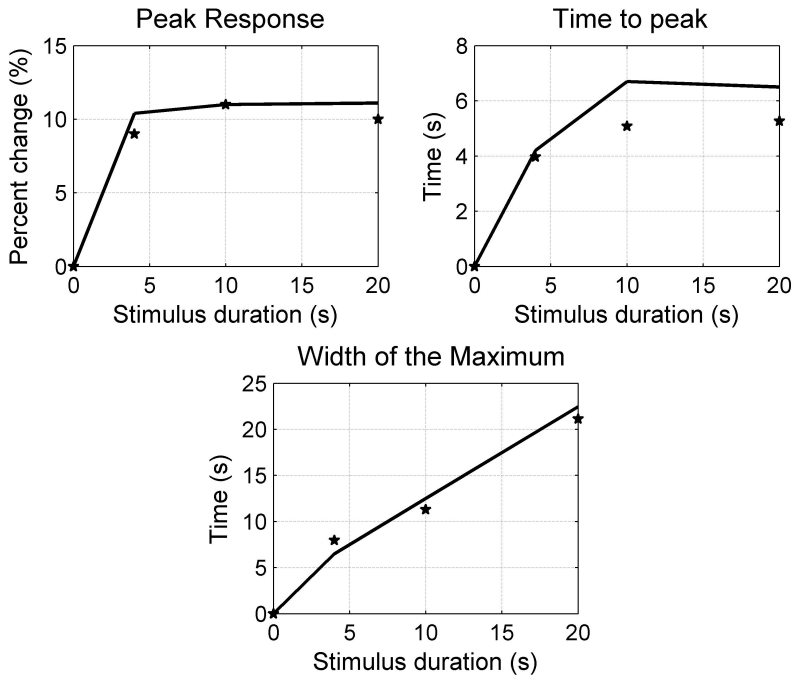

Figure 8.1 Percent change in peak response (A), time to peak to the peak response (B) and width of the maximum (C) with respect to stimulus duration. Modeling results: black curve and experimental data: stars.

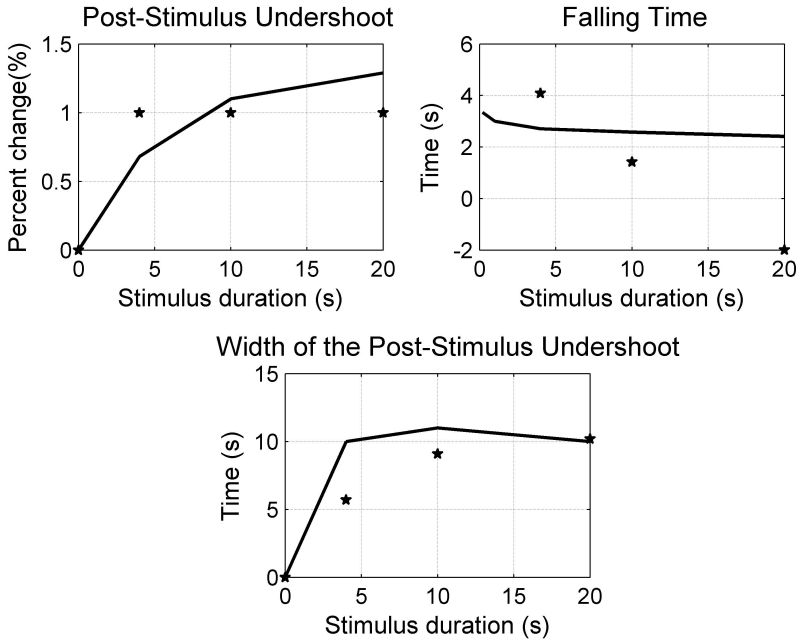

Figure 8.2 Post-stimulus undershoot percent change (A), falling time to the peak of the undershoot (B) and width of the undershoot (C) with respect to stimulus duration. Modeling results: black curve and experimental data: stars.

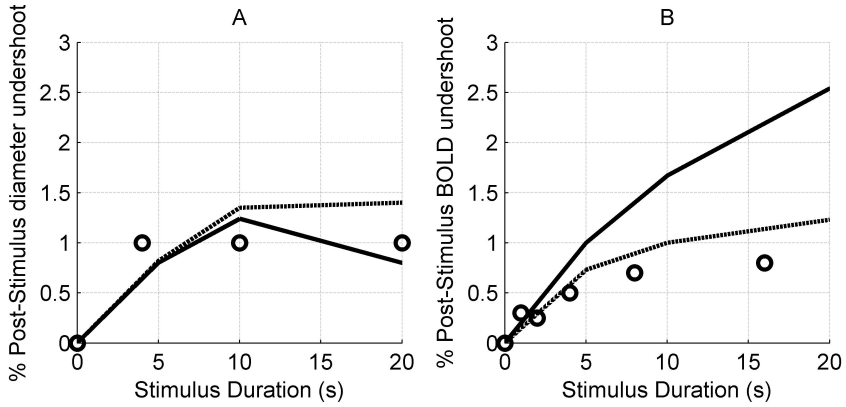

Figure 8.3 Minimum of the post-stimulus diameter undershoot versus stimulus duration (A). Post-stimulus BOLD undershoot versus stimulus duration (B). Experimental data from this work (circles in A), experimental data from literature given in Table 8.1 (circles in B), model results (solid line), model results when the model is forced to have a faster $CMRO_2$ increase following stimulus onset and recovery post-stimulus (dashed-line).

of the forced model is in a closer agreement with our experimental results.

In Figure 8.3B, we have shown the peak post-stimulus BOLD undershoots. In addition to our modeling result (solid-line), we also introduced the model results when the model is forced to have slow $CMRO_2$ onset and recovery kinetics (dashed-line). The experimental data points that we have added for comparison are from literature (please see Table 8.1). Similar to diameter results, BOLD results obtained with the forced model are in conformity with the experimental results. Overall our results support a fast $CMRO_2$ onset and recovery kinetics (in seconds), rather than a slow onset and recovery kinetics (in minutes).

Table 8.1
Peak % BOLD undershoot at various stimulus durations in literature.

Stimulus Duration (s)	% BOLD undershoot	Reference
1	0.3	[146]
2	0.25	[146]
4	0.5	[146]
8	0.7	[146]
16	0.8	[146]
32	1	[146]

9. DISCUSSION - EXPERIMENTS AND COMPARISON WITH THE MODEL

We investigated the dilation characteristics of the vessels in the activation area in response to forepaw stimulation at different stimulus durations with two-photon microscopy. We obtained statistically significant results which give more insight into the understanding of hemodynamic response to functional activity. The relatively high standard deviations of the results may be due to both the problems encountered during animal preparation and the difficulty in keeping the animal under normal physiological conditions, or just the normal variance of the physiological system.

The difference in the peak response percentage in two caliber groups (diameters smaller and larger than 40 μm) can have more than one explanation. One of the explanations relies on the fact that smaller vessels are located closer to the activation area considering the anatomical localization of the vessels, and closer the vessels to the activation area, larger the response considering the functional imaging data. Experimental evidence confirming this is given by Hillman et al. They have shown that closer to the activation area, the total hemoglobin change, which is assumed to represent total blood volume, is higher [147]. A second explanation is that the difference may be due to an intrinsic property of the vessel. The reactivity of the vascular diameter (in %/kPa) has been shown to increase going from larger to smaller baseline diameters [148]. Thirdly, according to a recent work on rats with *in vivo* microangiography, perforating arteries distend more efficiently than pial arteries: they dilate more when exposed to hypotension [149]. They give an anatomical explanation to this phenomenon: the pial arteries have two to three layers of smooth muscle, while penetrating arteries have only one to two layers so they are more elastic. Moreover it is shown in the same work that, smaller vessels, both cortical and perforating, dilate percent-wise significantly more than their larger counterparts.

Both our experimental results and modeling results show that the percent change in peak response is increasing up to 4 seconds of stimulus duration, while it remains unchanged for longer stimulus durations. The explanation from our model is that the neurogenically produced vasodilator, NO, reaches a steady state value a couple of seconds after the stimulus onset due to the balance of its production with its consumption and diffusion.

The first peak or the overshoot in dilation we observed in our experimental work also appears in our modeling results. Our model provides a novel explanation for an initial CBF overshoot during the first 10 s of a stimulus as observed by Krüger et al. (1999) arising from CO_2. If the model is given a habituating action potential as an input, the undershoot is enhanced. During the initial few seconds of the stimulus, the CBF response is dominated by the NO effect. This increase in CBF washes out CO_2, the vessels constrict slightly because of the reduced pCO_2, and thus CBF reduces slightly from the increased vascular resistance. Interestingly, closer inspection of our results for the longer duration stimulus (Figure 5.2C) shows a subsequent increase in CBF after reaching a minimum at 20 s, consistent with our experimental work or previous works from Hoge et al. and Krüger et al. [136, 150]. This secondary increase in CBF, according to our model, arises from oxygen consumption continuing to increase during the stimulus, producing more CO_2 (see Figure 5.4), dilating the vessels, and increasing CBF.

Our results show that there is a significant difference in time to peak values in two caliber groups, smaller diameter group having shorter time to peak values. This difference may be due to at least two different phenomena. The first one being the fact that smaller arterioles and capillaries are more elastic compared to their larger counterparts as previously mentioned [149]. The latter explanation is the retrograde dilation hypothesis, which can be briefly described as the fact that upon a local functional activity, dilation starts at the terminal arterioles and ascends into the proximal arterioles and feeding arteries upstream. This will result in a delay in dilation of the upstream arterioles which will show itself as a difference in time to peak values of the two vessel groups. However, in order to be able to claim a retrograde dilation from a

difference in time to peak values, one should also be able to show the same difference in the onset times of the two groups. Our results also show a difference in onset times of the groups, larger groups having a delay in response. Our results, thus, is in favor of the retrograde dilation hypothesis. A work by Chen et al on superficial cortical regions shows a longer delay in response between superficial and deep regions [9]. The difference may be due to the usage of two different imaging modalities in two works or with the fact that the vessels they measured in superficial regions are further away from the activation regions compared to our work.

Our modeling results, in conformity with our experimental results, show that the time to peak value first increases and reaches a steady state value with increasing stimulus duration. According to our modeling results this is directly related to the production and consumption of the neurogenically produced vasodilator NO. The lower values observed imply that the maximum NO concentration has not been achieved yet.

The widths of the dilation of the positive response are not significantly different between the smaller and larger diameter groups. However, the mean of the width of the undershoot is significantly longer for smaller diameter vessels for all stimulus durations. The difference maybe explained by the fact that the vasoconstrictive mechanism lasts longer in the activation area since the vessels nearby dilate more.

There is a significant difference in the widths of the positive dilation among different stimulus durations. The width increases with increasing stimulus duration. The width of the positive response is expected to be directly proportional to the duration of the stimulus, since the vasodilatory agents are being produced throughout the stimulus. Our modeling results are in good agreement with our experimental results. The width of the maximum, according to our model, is determined mostly by the neurogenic mediators rather than metabolic ones. This implies that the width of the dilation is determined solely by the duration of the neuronal activity.

We observed a post-stimulus undershoot both experimentally and by modeling approach. Although there is no direct evidence for a hypocapnic vasoconstrictive effect

of CO_2 washout during brain activation in the literature, our model provides a novel explanation for the features of CBF response observed in the literature. Our modeling approach provides a new explanation for this undershoot: the increase in CBF during the stimulus has washed-out more CO_2 than is being produced by the increased oxygen consumption. This reduces tissue pCO_2 such that when the NO vasodilation returns to baseline post-stimulus, the reduced pCO_2 results in vasoconstriction and an undershoot in CBF.

The post-stimulus undershoot percentage is significantly higher for the smaller diameter group. This is either due to the more elastic structure of the smaller vessels or due to the locally regulated constriction mechanisms which are more effective in the activation area or both.

No significant difference in the post-stimulus undershoot percentage is observed with changing stimulus duration in our experiments. Our model results based on slow $CMRO_2$ kinetics, on the other hand, shows first a peak and then a decrease in undershoot with increasing stimulus duration. The forced model which has faster $CMRO_2$ kinetics, in contrary, is in a closer agreement with our experimental results. The resultant post-stimulus behavior is determined by the co-effect of the production of a vasodilatory substance, in our model CO_2, and the wash-out of this agent by the cerebral blood flow increases. In the fast $CMRO_2$ kinetics scenario, the CO_2 production decreases faster so the peak seen in slow kinetics does not appear any more.

Falling time is calculated to measure possible differences in the recovery of the response with changing conditions, since it discards the duration of the stimulus. The falling time that we obtained is shorter than a work by Chen et al. [9]. The difference can be explained by the fact that we measure directly the dilation in arterioles and capillaries, while they measure CBV which may have a delay in recovery. The falling time is significantly longer for the larger diameter group for only 4 s stimulus. This may be explained by the local control of post-stimulus behaviors, which affects first the small vessels located at the center of the activation area. On the other hand, the falling time decreases significantly at longer stimulus durations for both caliber

size groups. Our modeling results are in conformity with the decrease with increasing stimulus duration. While the falling time obtained for up to 10 seconds are similar, the value is much lower for the experimental case.

The width of the post-stimulus undershoot is significantly longer for the smaller vessel group. A possible explanation for this is that vasoconstrictive mechanism lasts longer in the activation area, since the vessels nearby dilates more.

There is a significant difference in the widths of the post-stimulus undershoot among different stimulus durations. Both our modeling and experimental results show that the width of the undershoot first increases, and then reaches steady state when the stimulus duration is increased up to 20 seconds. This may be caused by the washing-out of an already existing vasoactive metabolite in the medium, in the case of our model: CO_2. The width reaches a steady-state value at the time maximum washing out is obtained by the coming blood flow.

We compared the post-stimulus BOLD signal we obtained by our model with experimental data from literature. We tried different $CMRO_2$ onset kinetics in our model to see the possible changes in our results. The BOLD percentage increase was lower for the fast kinetics than for the slow kinetics, and in better agreement with literature. However, the increasing kinetics for $CMRO_2$ did not have much of an effect on the CBF onset, and CBF post-stimulus transients.

10. CONCLUSION AND FUTURE WORK

In this work, we tried to provide new insights to various aspects of neurovascular coupling hypotheses with the help of mathematical modeling and experiments. While our modeling approach targeted to resolve the relative effects of neurogenic and metabolic factors on neurovascular coupling mechanism, our experimental design revealed whether the dilation was controlled locally or remotely. Our experimental findings revealed many other important features of the hemodynamic response. The comparison of the modeling and experimental results on post-stimulus dilation characteristics, and the comparison of the modeling results with the post-stimulus BOLD kinetics from literature gave more insight to the unresolved problem of $CMRO_2$ kinetics.

Our modeling results support the dominant vasodilatory role of NO, and indicates a modulatory role of CO_2 on the shape of the response, in particular the initial overshoot and the post-stimulus undershoot. The wash-out of CO_2 by the increased CBF levels results in a vasoconstrictive effect throughout the stimulus and in the period following it.

We observed an initial CBF overshoot during the first 10 seconds of the stimulus arising from CO_2 dynamics, and a second subsequent increase in CBF arising from oxygen consumption continuing to increase during the stimulus, producing more CO_2, so being less vasoconstrictive.

The results of the model with slow $CMRO_2$ onset and recovery kinetics for short duration stimulus (20 s) lead to a post-stimulus undershoot in CBF while we see only a very brief and small undershoot for the long duration (100 s) stimulus which is subsequently followed by a slow positive CBF recovery. The post-stimulus undershoot dynamics of short and long duration stimulus, however, are similar when the model is forced to have fast $CMRO_2$ onset and recovery kinetics. Our experimental results

also show no significant difference in the percent post-stimulus undershoot change with changing stimulus duration in accordance with our results with fast $CMRO_2$ kinetics. We should add that the CO_2 wash-out results in a similar vasoconstrictive effect in both slow and fast $CMRO_2$ kinetics.

A positive BOLD response is obtained throughout the stimulus when the effect of only NO and both NO and CO_2 are considered. Inhibiting the effect of NO, on the other hand, results in a negative BOLD response resulting from an insufficient oxygen supply to the activation area. Moreover, our model results support the combined roles of a flow undershoot and a sustained post-stimulus increase in $CMRO_2$ in producing a BOLD undershoot, with the former dominating for short-stimuli and the latter for longer duration stimuli. Trials of slow and fast $CMRO_2$ kinetics in our model indicate a lower BOLD % increase for the fast kinetics than for the slow kinetics.

Our experiments provided significant results in the dilation characteristics of the vessels in the activation area in response to forepaw stimulation at different stimulus durations. The results we obtained for the percent peak response change, time to peak and percent post-stimulus undershoot change show a clear grouping of the diameters, which led us to further consolidate our data into two groups: diameters smaller and larger than 40 μm.

Our major findings related to the stimulus duration dependency of the calculated parameters are: 1) there is no significant difference in peak response amplitude or in peak response percent change or in post-stimulus undershoot amplitude with changing stimulus durations, 2) time to peak values is shorter for 4 second stimulus compared to 10 and 20 second durations and it is almost constant for the stimulus durations longer than 4 second, 3) a significant difference in the width of the dilation is found among different stimulus durations, width being longer for longer stimulus durations 4) falling time significantly decreases at longer stimulus durations, 5) width of the undershoot increases with increasing stimulus duration, difference being significant for the smaller diameter group, and marginally significant for the larger diameter group. Our modeling results are in conformity with these experimental results and have the potential to

explain why these transients change as explained here with stimulus duration.

The main findings related to the baseline vessel diameter dependency of the calculated parameters are: 1) peak response amplitude is significantly higher for the larger vessel group 2) mean of the percent peak response for each stimulus duration is higher for the smaller diameter group, the variance being significant only for the 4 second stimulus and marginally significant for the 10 second stimulus, 3) larger vessels have around 1 second delay in time to peak values 4) small diameter group's increase is around 1.5 %, while larger diameter group's increase is only 0.5 % in the first 1.18 s of the stimulus onset 5) at 0.8 from stimulus onset, vessels larger than 50 μm do not start dilating at all 6) our findings in 3, 4, 5 mentioned above support retrograde dilation hypothesis, 7) there is no significant difference between the smaller and larger diameter groups in terms of the width of the dilation, 8) no significant difference is observed in post-stimulus undershoot amplitude with caliber size, 9) smaller diameter group has significantly higher percent post-stimulus undershoot, 10) falling time is significantly longer for the larger diameter group for 4 s stimulus and the variance is not significant for the 10 and 20 second stimulus durations, and 11) mean of the width of the undershoot is longer for smaller diameter vessels, the difference being insignificant.

Possible future works include the modification of the model so that it includes two vessels groups whose characteristics are defined by the results of the experimental work herein, and to extrapolate this model from a single neurovascular unit to a large scale which represents the whole brain. This approach is expected to be correlated with fMRI BOLD signal properly. The existing model can also be employed to see the hemodynamic response changes with changing stimulus frequency, which is the input to the model. It could be also interesting to extrapolate the model to see the metabolic profile in whole brain structure to see the effect of different $CMRO_2$ kinetics and compare it with $CMRO_2$ estimated by fMRI BOLD signal and PET studies. As of modeling improvements, other significant vasodilators and membrane channels those are active during neuronal activity, and the energy requirements related to post-synaptic potentials can also be added to the model.

APPENDIX A. Publications during PhD Studies

A.1 Peer-reviewed Journal Papers

Yücel, M. A., A. Devor, A. Akın and D. A. Boas (2009). "The possible role of CO_2 in producing a post-stimulus CBF and BOLD undershoot." Frontiers in Neuroenergetics, 1(7).

A.2 Conferences

Devor, A., S. Sakadzic, M. A. Yücel, I. C. Teng, K. A. Kasischke and D. A. Boas, "*In vivo* functional NADH imaging with single-cell resolution" Poster presentation in Society for Neuroscience, Chicago, IL, Oct, 2009.

Yücel, M. A., A. Devor, A. Akın and D. A. Boas, "A neurovascular coupling model investigating the relative contributions of metabolism-driven and synapse-driven vasodilation" Poster presentation in Society for Neuroscience, Washington DC, Nov, 2008.

Mesquita, R. C. , M. A. Yücel, A. Akın, A. Devor, T.J. Huppert and D.A. Boas, "Investigating neurovascular coupling in rat brain with optical imaging and physiological modeling" Poster presentation in Optics and Photonics Congress, St. Petersburg, FL, March, 2008.

Yücel, M. A., A. Akın and T. Demiralp. "NO and CO_2 in NVC." Poster Presentation in VI. Ulusal Sinirbilimleri Kongresi, Karabük, Turkey, April 2007.

REFERENCES

1. Kety, S. S., and C. F. Schmidt, "The determination of cerebral blood flow in man by the use of nitrous oxide in low concentrations.," *Am. J. Physiol.*, Vol. 143, pp. 53–66, 1945.

2. Grubb, R. L., M. E. Raichle, J. O. Eichling, and M. M. Ter-Pogossian, "The effects of changes in PaCO2 on cerebral blood volume, blood flow, and vascular mean transit time," *Stroke*, Vol. 5, pp. 630–639, 1974.

3. Hoge, R. D., J. Atkinson, B. Gill, G. R. Crelier, S. Marrett, and G. B. Pike, "Linear coupling between cerebral blood flow and oxygen consumption in activated human cortex," *Proc. Natl. Acad. Sci. U.S.A.*, Vol. 96, pp. 9403–9408, Aug 1999.

4. Girouard, H., and C. Iadecola, "Neurovascular coupling in the normal brain and in hypertension, stroke, and Alzheimer disease," *J. Appl. Physiol.*, Vol. 100, pp. 328–335, Jan 2006.

5. Estrada, C., and J. DeFelipe, "Nitric oxide-producing neurons in the neocortex: morphological and functional relationship with intraparenchymal microvasculature," *Cereb. Cortex*, Vol. 8, pp. 193–203, 1998.

6. Riera, J. J., A. Schousboe, H. S. Waagepetersen, C. Howarth, and F. Hyder, "The micro-architecture of the cerebral cortex: functional neuroimaging models and metabolism," *Neuroimage*, Vol. 40, pp. 1436–1459, May 2008.

7. Ito, H., I. Kanno, and H. Fukuda, "Human cerebral circulation: positron emission tomography studies," *Ann Nucl Med*, Vol. 19, pp. 65–74, Apr 2005.

8. Segal, S. S., "Regulation of blood flow in the microcirculation," *Microcirculation*, Vol. 12, pp. 33–45, 2005.

9. Chen, Y., A. D. Aguirre, L. Ruvinskaya, A. Devor, D. A. Boas, and J. G. Fujimoto, "Optical coherence tomography (OCT) reveals depth-resolved dynamics during functional brain activation," *J. Neurosci. Methods*, Vol. 178, pp. 162–173, Mar 2009.

10. Mintun, M. A., A. G. Vlassenko, G. L. Shulman, and A. Z. Snyder, "Time-related increase of oxygen utilization in continuously activated human visual cortex," *Neuroimage*, Vol. 16, pp. 531–537, Jun 2002.

11. Davis, T. L., K. K. Kwong, R. M. Weisskoff, and B. R. Rosen, "Calibrated functional MRI: mapping the dynamics of oxidative metabolism," *Proc. Natl. Acad. Sci. U.S.A.*, Vol. 95, pp. 1834–1839, Feb 1998.

12. Maciejewski, P. K., I. Kida, and F. Hyder, "Estimating dynamic CMRO2 from dynamic CBF and BOLD fMRI measurements.," *Proc Intl Soc Mag Reson*, Vol. 11, 2004.

13. Shen, Q., H. Ren, and T. Q. Duong, "CBF, BOLD, CBV, and CMRO(2) fMRI signal temporal dynamics at 500-msec resolution," *J Magn Reson Imaging*, Vol. 27, pp. 599–606, Mar 2008.

14. Wu, C. W., H. Gu, H. Lu, E. A. Stein, J. H. Chen, and Y. Yang, "Mapping functional connectivity based on synchronized CMRO2 fluctuations during the resting state," *Neuroimage*, Vol. 45, pp. 694–701, Apr 2009.

15. Raichle, M. E., and M. A. Mintun, "Brain work and brain imaging," *Annu. Rev. Neurosci.*, Vol. 29, pp. 449–476, 2006.

16. Roy, C. S., and C. S. Sherrington, "On the Regulation of the Blood-supply of the Brain," *J. Physiol. (Lond.)*, Vol. 11, pp. 85–158, Jan 1890.

17. Lok, J., P. Gupta, S. Guo, W. J. Kim, M. J. Whalen, K. van Leyen, and E. H. Lo, "Cell-cell signaling in the neurovascular unit," *Neurochem. Res.*, Vol. 32, pp. 2032–2045, Dec 2007.

18. Magistretti, P., "Brain energy metabolism," in *Fundamental Neuroscience*, San Diego, CA: Elsevier Science, 2nd ed., 2003.

19. Sokoloff, L., M. Reivich, C. Kennedy, M. H. Des Rosiers, C. S. Patlak, K. D. Pettigrew, O. Sakurada, and M. Shinohara, "The [14C]deoxyglucose method for the measurement of local cerebral glucose utilization: theory, procedure, and normal values in the conscious and anesthetized albino rat," *J. Neurochem.*, Vol. 28, pp. 897–916, May 1977.

20. Sokoloff, L., "Localization of functional activity in the central nervous system by measurement of glucose utilization with radioactive deoxyglucose," *J. Cereb. Blood Flow Metab.*, Vol. 1, pp. 7–36, 1981.

21. Gjedde, A., S. Marrett, and M. Vafaee, "Oxidative and nonoxidative metabolism of excited neurons and astrocytes," *J. Cereb. Blood Flow Metab.*, Vol. 22, pp. 1–14, Jan 2002.

22. Marrett, S., and A. Gjedde, "Changes of blood flow and oxygen consumption in visual cortex of living humans," *Adv. Exp. Med. Biol.*, Vol. 413, pp. 205–208, 1997.

23. Fox, P. T., M. E. Raichle, M. A. Mintun, and C. Dence, "Nonoxidative glucose consumption during focal physiologic neural activity," *Science*, Vol. 241, pp. 462–464, Jul 1988.

24. Attwell, D., and S. B. Laughlin, "An energy budget for signaling in the grey matter of the brain," *J. Cereb. Blood Flow Metab.*, Vol. 21, pp. 1133–1145, Oct 2001.

25. Skou, J. C., "The influence of some cations on an adenosine triphosphatase from peripheral nerves," *Biochim. Biophys. Acta*, Vol. 23, pp. 394–401, Feb 1957.

26. Proverbio, F., and J. F. Hoffman, "Membrane compartmentalized ATP and its preferential use by the Na,K-ATPase of human red cell ghosts," *J. Gen. Physiol.*, Vol. 69, pp. 605–632, May 1977.

27. van den Berg, C. J., and D. Garfinkel, "A stimulation study of brain compartments. Metabolism of glutamate and related substances in mouse brain," *Biochem. J.*, Vol. 123, pp. 211–218, Jun 1971.

28. Bröer, S., and N. Brookes, "Transfer of glutamine between astrocytes and neurons," *J. Neurochem.*, Vol. 77, pp. 705–719, May 2001.

29. Pellerin, L., and P. J. Magistretti, "Glutamate uptake into astrocytes stimulates aerobic glycolysis: a mechanism coupling neuronal activity to glucose utilization," *Proc. Natl. Acad. Sci. U.S.A.*, Vol. 91, pp. 10625–10629, Oct 1994.

30. Magistretti, P. J., L. Pellerin, D. L. Rothman, and R. G. Shulman, "Energy on demand," *Science*, Vol. 283, pp. 496–497, Jan 1999.

31. Sibson, N. R., A. Dhankhar, G. F. Mason, D. L. Rothman, K. L. Behar, and R. G. Shulman, "Stoichiometric coupling of brain glucose metabolism and glutamatergic neuronal activity," *Proc. Natl. Acad. Sci. U.S.A.*, Vol. 95, pp. 316–321, Jan 1998.

32. Bouzier-Sore, A. K., P. Voisin, P. Canioni, P. J. Magistretti, and L. Pellerin, "Lactate is a preferential oxidative energy substrate over glucose for neurons in culture," *J. Cereb. Blood Flow Metab.*, Vol. 23, pp. 1298–1306, Nov 2003.

33. Poitry-Yamate, C. L., S. Poitry, and M. Tsacopoulos, "Lactate released by Müller glial cells is metabolized by photoreceptors from mammalian retina," *J. Neurosci.*, Vol. 15, pp. 5179–5191, Jul 1995.

34. Bak, L. K., A. Schousboe, U. Sonnewald, and H. S. Waagepetersen, "Glucose is necessary to maintain neurotransmitter homeostasis during synaptic activity in cultured glutamatergic neurons," *J. Cereb. Blood Flow Metab.*, Vol. 26, pp. 1285–1297, Oct 2006.

35. Mangia, S., F. Giove, I. TkÃ¡c, N. K. Logothetis, P. G. Henry, C. A. Olman, B. Maraviglia, F. Di Salle, and K. UÄurbil, "Metabolic and hemodynamic events after changes in neuronal activity: current hypotheses, theoretical predictions and in vivo NMR experimental findings," *J. Cereb. Blood Flow Metab.*, Vol. 29, pp. 441–463, Mar 2009.

36. Kasischke, K. A., H. D. Vishwasrao, P. J. Fisher, W. R. Zipfel, and W. W. Webb, "Neural activity triggers neuronal oxidative metabolism followed by astrocytic glycolysis," *Science*, Vol. 305, pp. 99–103, Jul 2004.

37. Simpson, I. A., A. Carruthers, and S. J. Vannucci, "Supply and demand in cerebral energy metabolism: the role of nutrient transporters," *J. Cereb. Blood Flow Metab.*, Vol. 27, pp. 1766–1791, Nov 2007.

38. Lu, H., X. Golay, J. J. Pekar, and P. C. Van Zijl, "Sustained poststimulus elevation in cerebral oxygen utilization after vascular recovery," *J. Cereb. Blood Flow Metab.*, Vol. 24, pp. 764–770, Jul 2004.

39. Gsell, W., C. De Sadeleer, Y. Marchalant, E. T. MacKenzie, P. Schumann, and F. Dauphin, "The use of cerebral blood flow as an index of neuronal activity in functional neuroimaging: experimental and pathophysiological considerations," *J. Chem. Neuroanat.*, Vol. 20, pp. 215–224, Dec 2000.

40. Fox, P. T., and M. E. Raichle, "Focal physiological uncoupling of cerebral blood flow and oxidative metabolism during somatosensory stimulation in human subjects," *Proc. Natl. Acad. Sci. U.S.A.*, Vol. 83, pp. 1140–1144, Feb 1986.

41. Shimojyo, S., P. Scheinberg, K. Kogure, and O. M. Reinmuth, "The effects of graded hypoxia upon transient cerebral blood flow and oxygen consumption," *Neurology*, Vol. 18, pp. 127–133, Feb 1968.

42. Wolf, T., U. Lindauer, A. Villringer, and U. Dirnagl, "Excessive oxygen or glucose supply does not alter the blood flow response to somatosensory stimulation or spreading depression in rats," *Brain Res.*, Vol. 761, pp. 290–299, Jul 1997.

43. Kofuji, P., and E. A. Newman, "Potassium buffering in the central nervous system," *Neuroscience*, Vol. 129, pp. 1045–1056, 2004.

44. Metea, M. R., and E. A. Newman, "Signalling within the neurovascular unit in the mammalian retina," *Exp. Physiol.*, Vol. 92, pp. 635–640, Jul 2007.

45. Brockhaus, J., K. Ballanyi, J. C. Smith, and D. W. Richter, "Microenvironment of respiratory neurons in the in vitro brainstem-spinal cord of neonatal rats," *J. Physiol. (Lond.)*, Vol. 462, pp. 421–445, Mar 1993.

46. Newman, E. A., "New roles for astrocytes: regulation of synaptic transmission," *Trends Neurosci.*, Vol. 26, pp. 536–542, Oct 2003.

47. Markus, H. S., "Cerebral perfusion and stroke," *J. Neurol. Neurosurg. Psychiatr.*, Vol. 75, pp. 353–361, Mar 2004.

48. Lauritzen, M., "Reading vascular changes in brain imaging: is dendritic calcium the key?," *Nat. Rev. Neurosci.*, Vol. 6, pp. 77–85, Jan 2005.

49. Kontos, H. A., E. P. Wei, A. J. Raper, and J. L. Patterson, "Local mechanism of CO2 action of cat pial arterioles," *Stroke*, Vol. 8, pp. 226–229, 1977.

50. Chen, Q., and D. R. Anderson, "Effect of CO2 on intracellular pH and contraction of retinal capillary pericytes," *Invest. Ophthalmol. Vis. Sci.*, Vol. 38, pp. 643–651, Mar 1997.

51. Wagerle, L. C., and O. P. Mishra, "Mechanism of CO2 response in cerebral arteries of the newborn pig: role of phospholipase, cyclooxygenase, and lipoxygenase pathways," *Circ. Res.*, Vol. 62, pp. 1019–1026, May 1988.

52. Ursino, M., and C. A. Lodi, "Interaction among autoregulation, CO2 reactivity, and intracranial pressure: a mathematical model," *Am. J. Physiol.*, Vol. 274, pp. H1715–1728, May 1998.

53. Ursino, M., A. Ter Minassian, C. A. Lodi, and L. Beydon, "Cerebral hemodynamics during arterial and CO(2) pressure changes: in vivo prediction by a mathematical model," *Am. J. Physiol. Heart Circ. Physiol.*, Vol. 279, pp. H2439–2455, Nov 2000.

54. Payne, S. J., "A model of the interaction between autoregulation and neural activation in the brain," *Math Biosci*, Vol. 204, pp. 260–281, Dec 2006.

55. Buxton, R. B., and L. R. Frank, "A model for the coupling between cerebral blood flow and oxygen metabolism during neural stimulation," *J. Cereb. Blood Flow Metab.*, Vol. 17, pp. 64–72, Jan 1997.

56. Buxton, R. B., E. C. Wong, and L. R. Frank, "Dynamics of blood flow and oxygenation changes during brain activation: the balloon model," *Magn Reson Med*, Vol. 39, pp. 855–864, Jun 1998.

57. Mandeville, J. B., J. J. Marota, C. Ayata, G. Zaharchuk, M. A. Moskowitz, B. R. Rosen, and R. M. Weisskoff, "Evidence of a cerebrovascular postarteriole windkessel with delayed compliance," *J. Cereb. Blood Flow Metab.*, Vol. 19, pp. 679–689, Jun 1999.

58. Zheng, Y., J. Martindale, D. Johnston, M. Jones, J. Berwick, and J. Mayhew, "A model of the hemodynamic response and oxygen delivery to brain," *Neuroimage*, Vol. 16, pp. 617–637, Jul 2002.

59. Toda, N., K. Ayajiki, and T. Okamura, "Cerebral blood flow regulation by nitric oxide in neurological disorders," *Can. J. Physiol. Pharmacol.*, Vol. 87, pp. 581–594, Aug 2009.

60. Furchgott, R. F., and J. V. Zawadzki, "The obligatory role of endothelial cells in the relaxation of arterial smooth muscle by acetylcholine," *Nature*, Vol. 288, pp. 373–376, Nov 1980.

61. Bredt, D. S., C. E. Glatt, P. M. Hwang, M. Fotuhi, T. M. Dawson, and S. H. Snyder, "Nitric oxide synthase protein and mRNA are discretely localized in neuronal populations of the mammalian CNS together with NADPH diaphorase," *Neuron*, Vol. 7, pp. 615–624, Oct 1991.

62. Ayata, C., J. Ma, W. Meng, P. Huang, and M. A. Moskowitz, "L-NA-sensitive rCBF augmentation during vibrissal stimulation in type III nitric oxide synthase mutant mice," *J. Cereb. Blood Flow Metab.*, Vol. 16, pp. 539–541, Jul 1996.

63. Buerk, D. G., C. E. Riva, and S. D. Cranstoun, "Nitric oxide has a vasodilatory role in cat optic nerve head during flicker stimuli," *Microvasc. Res.*, Vol. 52, pp. 13–26, Jul 1996.

64. Buerk, D. G., B. M. Ances, J. H. Greenberg, and J. A. Detre, "Temporal dynamics of brain tissue nitric oxide during functional forepaw stimulation in rats," *Neuroimage*, Vol. 18, pp. 1–9, Jan 2003.

65. Cholet, N., J. Seylaz, P. Lacombe, and G. Bonvento, "Local uncoupling of the cerebrovascular and metabolic responses to somatosensory stimulation after neuronal nitric oxide synthase inhibition," *J. Cereb. Blood Flow Metab.*, Vol. 17, pp. 1191–1201, Nov 1997.

66. Lindauer, U., D. Megow, H. Matsuda, and U. Dirnagl, "Nitric oxide: a modulator, but not a mediator, of neurovascular coupling in rat somatosensory cortex," *Am. J. Physiol.*, Vol. 277, pp. 799–811, Aug 1999.

67. Yang, G., G. Chen, T. J. Ebner, and C. Iadecola, "Nitric oxide is the predominant mediator of cerebellar hyperemia during somatosensory activation in rats," *Am. J. Physiol.*, Vol. 277, pp. R1760–1770, Dec 1999.

68. Stefanovic, B., W. Schwindt, M. Hoehn, and A. C. Silva, "Functional uncoupling of hemodynamic from neuronal response by inhibition of neuronal nitric oxide synthase," *J. Cereb. Blood Flow Metab.*, Vol. 27, pp. 741–754, Apr 2007.

69. Akgören, N., M. Fabricius, and M. Lauritzen, "Importance of nitric oxide for local increases of blood flow in rat cerebellar cortex during electrical stimulation," *Proc. Natl. Acad. Sci. U.S.A.*, Vol. 91, pp. 5903–5907, Jun 1994.

70. Yang, G., Y. Zhang, M. E. Ross, and C. Iadecola, "Attenuation of activity-induced increases in cerebellar blood flow in mice lacking neuronal nitric oxide synthase," *Am. J. Physiol. Heart Circ. Physiol.*, Vol. 285, pp. 298–304, Jul 2003.

71. Bredt, D. S., and S. H. Snyder, "Nitric oxide mediates glutamate-linked enhancement of cGMP levels in the cerebellum," *Proc. Natl. Acad. Sci. U.S.A.*, Vol. 86, pp. 9030–9033, Nov 1989.

72. Garthwaite, J., G. Garthwaite, R. M. Palmer, and S. Moncada, "NMDA receptor activation induces nitric oxide synthesis from arginine in rat brain slices," *Eur. J. Pharmacol.*, Vol. 172, pp. 413–416, Oct 1989.

73. Palmer, R. M., D. S. Ashton, and S. Moncada, "Vascular endothelial cells synthesize nitric oxide from L-arginine," *Nature*, Vol. 333, pp. 664–666, Jun 1988.

74. Ledo, A., R. M. Barbosa, G. A. Gerhardt, E. Cadenas, and J. Laranjinha, "Concentration dynamics of nitric oxide in rat hippocampal subregions evoked by stimulation of the NMDA glutamate receptor," *Proc. Natl. Acad. Sci. U.S.A.*, Vol. 102, pp. 17483–17488, Nov 2005.

75. Esplugues, J. V., "NO as a signalling molecule in the nervous system," *Br. J. Pharmacol.*, Vol. 135, pp. 1079–1095, Mar 2002.

76. Murad, F., "Shattuck Lecture. Nitric oxide and cyclic GMP in cell signaling and drug development," *N. Engl. J. Med.*, Vol. 355, pp. 2003–2011, Nov 2006.

77. Buerk, D. G., "Can we model nitric oxide biotransport? A survey of mathematical models for a simple diatomic molecule with surprisingly complex biological activities," *Annu Rev Biomed Eng*, Vol. 3, pp. 109–143, 2001.

78. Seraya, I. P., and Y. R. Nartsissov, "Theoretical approach to description of time-dependent nitric oxide effects in the vasculature," *Mol. Biol. Rep.*, Vol. 29, pp. 151–155, 2002.

79. Chen, X., D. G. Buerk, K. A. Barbee, and D. Jaron, "A model of NO/O2 transport in capillary-perfused tissue containing an arteriole and venule pair," *Ann Biomed Eng*, Vol. 35, pp. 517–529, Apr 2007.

80. Wang, Q., D. A. Pelligrino, V. L. Baughman, H. M. Koenig, and R. F. Albrecht, "The role of neuronal nitric oxide synthase in regulation of cerebral blood flow in normocapnia and hypercapnia in rats," *J. Cereb. Blood Flow Metab.*, Vol. 15, pp. 774–778, Sep 1995.

81. White, R. P., C. Deane, P. Vallance, and H. S. Markus, "Nitric oxide synthase inhibition in humans reduces cerebral blood flow but not the hyperemic response to hypercapnia," *Stroke*, Vol. 29, pp. 467–472, Feb 1998.

82. Ances, B. M., J. H. Greenberg, and J. A. Detre, "The effects of graded hypercapnia on the activation flow coupling response due to forepaw stimulation in alpha-chloralose anesthetized rats," *Brain Res.*, Vol. 911, pp. 82–88, Aug 2001.

83. Aubert, A., and R. Costalat, "A model of the coupling between brain electrical activity, metabolism, and hemodynamics: application to the interpretation of functional neuroimaging," *Neuroimage*, Vol. 17, pp. 1162–1181, Nov 2002.

84. Aubert, A., and R. Costalat, "Interaction between astrocytes and neurons studied using a mathematical model of compartmentalized energy metabolism," *J. Cereb. Blood Flow Metab.*, Vol. 25, pp. 1476–1490, Nov 2005.

85. Banaji, M., I. Tachtsidis, D. Delpy, and S. Baigent, "A physiological model of cerebral blood flow control," *Math Biosci*, Vol. 194, pp. 125–173, Apr 2005.

86. Krogh, A., "The supply of oxygen to the tissues and the regulation of the capillary circulation," *J. Physiol. (Lond.)*, Vol. 52, pp. 457–474, May 1919.

87. Duling, B. R., and R. M. Berne, "Propagated vasodilation in the microcirculation of the hamster cheek pouch," *Circ. Res.*, Vol. 26, pp. 163–170, Feb 1970.

88. Dietrich, H. H., Y. Kajita, and R. G. Dacey, "Local and conducted vasomotor responses in isolated rat cerebral arterioles," *Am. J. Physiol.*, Vol. 271, pp. H1109–1116, Sep 1996.

89. Hilton, S. M., "A peripheral arterial conducting mechanism underlying dilatation of the femoral artery and concerned in functional vasodilatation in skeletal muscle," *J. Physiol. (Lond.)*, Vol. 149, pp. 93–111, Dec 1959.

90. Beach, J. M., E. D. McGahren, and B. R. Duling, "Capillaries and arterioles are electrically coupled in hamster cheek pouch," *Am. J. Physiol.*, Vol. 275, pp. H1489–1496, Oct 1998.

91. Sokoya, E. M., A. R. Burns, C. T. Setiawan, H. A. Coleman, H. C. Parkington, and M. Tare, "Evidence for the involvement of myoendothelial gap junctions in EDHF-mediated relaxation in the rat middle cerebral artery," *Am. J. Physiol. Heart Circ. Physiol.*, Vol. 291, pp. H385–393, Jul 2006.

92. Segal, S. S., "Cell-to-cell communication coordinates blood flow control," *Hypertension*, Vol. 23, pp. 1113–1120, Jun 1994.

93. Iadecola, C., G. Yang, T. J. Ebner, and G. Chen, "Local and propagated vascular responses evoked by focal synaptic activity in cerebellar cortex," *J. Neurophysiol.*, Vol. 78, pp. 651–659, Aug 1997.

94. Lin, A. L., P. T. Fox, Y. Yang, H. Lu, L. H. Tan, and J. H. Gao, "Time-dependent correlation of cerebral blood flow with oxygen metabolism in activated human visual cortex as measured by fMRI," *Neuroimage*, Vol. 44, pp. 16–22, Jan 2009.

95. Prichard, J., D. Rothman, E. Novotny, O. Petroff, T. Kuwabara, M. Avison, A. Howseman, C. Hanstock, and R. Shulman, "Lactate rise detected by 1H NMR in human visual cortex during physiologic stimulation," *Proc. Natl. Acad. Sci. U.S.A.*, Vol. 88, pp. 5829–5831, Jul 1991.

96. Nagaoka, T., F. Zhao, P. Wang, N. Harel, R. P. Kennan, S. Ogawa, and S. G. Kim, "Increases in oxygen consumption without cerebral blood volume change during visual stimulation under hypotension condition," *J. Cereb. Blood Flow Metab.*, Vol. 26, pp. 1043–1051, Aug 2006.

97. Zappe, A. C., K. Uludağ, and N. K. Logothetis, "Direct measurement of oxygen extraction with fMRI using 6Reson Imaging, Vol. 26, pp. 961–967, Sep 2008.

98. Aubert, A., L. Pellerin, P. J. Magistretti, and R. Costalat, "A coherent neurobiological framework for functional neuroimaging provided by a model integrating compartmentalized energy metabolism," *Proc. Natl. Acad. Sci. U.S.A.*, Vol. 104, pp. 4188–4193, Mar 2007.

99. Toda, N., and T. Okamura, "Cerebral vasodilators," *Jpn. J. Pharmacol.*, Vol. 76, pp. 349–367, Apr 1998.

100. Gros, G., and W. Moll, "The diffusion of carbon dioxide in erythrocytes and hemoglobin solutions," *Pflugers Arch.*, Vol. 324, pp. 249–266, 1971.

101. Lumb, A. B., *Nunn's Applied Respiratory Physiology*, Butterworth-Heinemann, 5nd ed., 2000.

102. Majewska, A., E. Brown, J. Ross, and R. Yuste, "Mechanisms of calcium decay kinetics in hippocampal spines: role of spine calcium pumps and calcium diffusion through the spine neck in biochemical compartmentalization," *J. Neurosci.*, Vol. 20, pp. 1722–1734, Mar 2000.

103. Kavdia, M., and A. S. Popel, "Contribution of nNOS- and eNOS-derived NO to microvascular smooth muscle NO exposure," *J. Appl. Physiol.*, Vol. 97, pp. 293–301, Jul 2004.

104. Vaughn, M. W., L. Kuo, and J. C. Liao, "Effective diffusion distance of nitric oxide in the microcirculation," *Am. J. Physiol.*, Vol. 274, pp. H1705–1714, May 1998.

105. Wada, T., M. D. McKee, S. Steitz, and C. M. Giachelli, "Calcification of vascular smooth muscle cell cultures: inhibition by osteopontin," *Circ. Res.*, Vol. 84, pp. 166–178, Feb 1999.

106. Cabrales, P., A. G. Tsai, R. M. Winslow, and M. Intaglietta, "Effects of extreme hemodilution with hemoglobin-based O2 carriers on microvascular pressure," *Am. J. Physiol. Heart Circ. Physiol.*, Vol. 288, pp. H2146–2153, May 2005.

107. Robert, A., and J. Freitas, *Nanomedicine, Basic Capabilities*, Georgetown, TX: Landes Bioscience, 1999.

108. Bronzino, J. D., ed., *The Biomedical Engineering Handbook*, Boca Raton, FL: CRC Press, 2000.

109. Huppert, T. J., M. S. Allen, H. Benav, P. B. Jones, and D. A. Boas, "A multicompartment vascular model for inferring baseline and functional changes in cerebral oxygen metabolism and arterial dilation," *J. Cereb. Blood Flow Metab.*, Vol. 27, pp. 1262–1279, Jun 2007.

110. Vafaee, M. S., and A. Gjedde, "Model of blood-brain transfer of oxygen explains nonlinear flow-metabolism coupling during stimulation of visual cortex," *J. Cereb. Blood Flow Metab.*, Vol. 20, pp. 747–754, Apr 2000.

111. Pasley, B. N., B. A. Inglis, and R. D. Freeman, "Analysis of oxygen metabolism implies a neural origin for the negative BOLD response in human visual cortex," *Neuroimage*, Vol. 36, pp. 269–276, Jun 2007.

112. Bean, B. P., "The action potential in mammalian central neurons," *Nat. Rev. Neurosci.*, Vol. 8, pp. 451–465, Jun 2007.

113. Hodgkin, A. L., and A. F. Huxley, "A quantitative description of membrane current and its application to conduction and excitation in nerve," *J. Physiol. (Lond.)*, Vol. 117, pp. 500–544, Aug 1952.

114. Shouval, H. Z., M. F. Bear, and L. N. Cooper, "A unified model of NMDA receptor-dependent bidirectional synaptic plasticity," *Proc. Natl. Acad. Sci. U.S.A.*, Vol. 99, pp. 10831–10836, Aug 2002.

115. Holzhütter, H. G., W. Henke, W. Dubiel, and G. Gerber, "A mathematical model to study short-term regulation of mitochondrial energy transduction," *Biochim. Biophys. Acta*, Vol. 810, pp. 252–268, Nov 1985.

116. Takahashi, S., and M. E. Mendelsohn, "Calmodulin-dependent and -independent activation of endothelial nitric-oxide synthase by heat shock protein 90," *J. Biol. Chem.*, Vol. 278, pp. 9339–9344, Mar 2003.

117. Luiking, Y. C., and N. E. Deutz, "Isotopic investigation of nitric oxide metabolism in disease," *Curr Opin Clin Nutr Metab Care*, Vol. 6, pp. 103–108, Jan 2003.

118. Yang, J., J. W. Clark, R. M. Bryan, and C. S. Robertson, "Mathematical modeling of the nitric oxide/cGMP pathway in the vascular smooth muscle cell," *Am. J. Physiol. Heart Circ. Physiol.*, Vol. 289, pp. H886–897, Aug 2005.

119. Wang, Q., O. B. Paulson, and N. A. Lassen, "Effect of nitric oxide blockade by NG-nitro-L-arginine on cerebral blood flow response to changes in carbon dioxide tension," *J. Cereb. Blood Flow Metab.*, Vol. 12, pp. 947–953, Nov 1992.

120. Muizelaar, J. P., H. G. van der Poel, Z. C. Li, H. A. Kontos, and J. E. Levasseur, "Pial arteriolar vessel diameter and CO2 reactivity during prolonged hyperventilation in the rabbit," *J. Neurosurg.*, Vol. 69, pp. 923–927, Dec 1988.

121. Schuster, A., H. Oishi, J. L. Bény, N. Stergiopulos, and J. J. Meister, "Simultaneous arterial calcium dynamics and diameter measurements: application to myoendothelial communication," *Am. J. Physiol. Heart Circ. Physiol.*, Vol. 280, pp. H1088–1096, Mar 2001.

122. Boas, D. A., G. Strangman, J. P. Culver, R. D. Hoge, G. Jasdzewski, R. A. Poldrack, B. R. Rosen, and J. B. Mandeville, "Can the cerebral metabolic rate of oxygen be estimated with near-infrared spectroscopy?," *Phys Med Biol*, Vol. 48, pp. 2405–2418, Aug 2003.

123. Malinow, R., N. Otmakhov, K. I. Blum, and J. Lisman, "Visualizing hippocampal synaptic function by optical detection of Ca2+ entry through the N-methyl-D-aspartate channel," *Proc. Natl. Acad. Sci. U.S.A.*, Vol. 91, pp. 8170–8174, Aug 1994.

124. Müller, W., and J. A. Connor, "Dendritic spines as individual neuronal compartments for synaptic Ca2+ responses," *Nature*, Vol. 354, pp. 73–76, Nov 1991.

125. Alford, S., B. G. Frenguelli, J. G. Schofield, and G. L. Collingridge, "Characterization of Ca2+ signals induced in hippocampal CA1 neurones by the synaptic activation of NMDA receptors," *J. Physiol. (Lond.)*, Vol. 469, pp. 693–716, Sep 1993.

126. Göbel, W., and F. Helmchen, "In vivo calcium imaging of neural network function," *Physiology (Bethesda)*, Vol. 22, pp. 358–365, Dec 2007.

127. Geers, C., and G. Gros, "Carbon dioxide transport and carbonic anhydrase in blood and muscle," *Physiol. Rev.*, Vol. 80, pp. 681–715, Apr 2000.

128. Meyer, E., C. O. Müller, and P. Fromherz, "Cable properties of dendrites in hippocampal neurons of the rat mapped by a voltage-sensitive dye," *Eur. J. Neurosci.*, Vol. 9, pp. 778–785, Apr 1997.

129. Morikawa, E., S. Rosenblatt, and M. A. Moskowitz, "L-arginine dilates rat pial arterioles by nitric oxide-dependent mechanisms and increases blood flow during focal cerebral ischaemia," *Br. J. Pharmacol.*, Vol. 107, pp. 905–907, Dec 1992.

130. Iadecola, C., and M. Nedergaard, "Glial regulation of the cerebral microvasculature," *Nat. Neurosci.*, Vol. 10, pp. 1369–1376, Nov 2007.

131. Kimura, S., S. Uchiyama, H. E. Takahashi, and K. Shibuki, "cAMP-dependent long-term potentiation of nitric oxide release from cerebellar parallel fibers in rats," *J. Neurosci.*, Vol. 18, pp. 8551–8558, Nov 1998.

132. Wu, W. C., Y. Wang, L. S. Kao, F. I. Tang, and C. Y. Chai, "Nitric oxide reduces blood pressure in the nucleus tractus solitarius: a real time electrochemical study," *Brain Res. Bull.*, Vol. 57, pp. 171–177, Jan 2002.

133. Lindauer, U., A. Villringer, and U. Dirnagl, "Characterization of CBF response to somatosensory stimulation: model and influence of anesthetics," *Am. J. Physiol.*, Vol. 264, pp. H1223–1228, Apr 1993.

134. Kida, I., D. L. Rothman, and F. Hyder, "Dynamics of changes in blood flow, volume, and oxygenation: implications for dynamic functional magnetic resonance imaging calibration," *J. Cereb. Blood Flow Metab.*, Vol. 27, pp. 690–696, Apr 2007.

135. Jin, T., and S. G. Kim, "Cortical layer-dependent dynamic blood oxygenation, cerebral blood flow and cerebral blood volume responses during visual stimulation," *Neuroimage*, Vol. 43, pp. 1–9, Oct 2008.

136. Hoge, R. D., J. Atkinson, B. Gill, G. R. Crelier, S. Marrett, and G. B. Pike, "Stimulus-dependent BOLD and perfusion dynamics in human V1," *Neuroimage*, Vol. 9, pp. 573–585, Jun 1999.

137. Kim, S. G., E. Rostrup, H. B. Larsson, S. Ogawa, and O. B. Paulson, "Determination of relative CMRO2 from CBF and BOLD changes: significant increase of oxygen consumption rate during visual stimulation," *Magn Reson Med*, Vol. 41, pp. 1152–1161, Jun 1999.

138. Uludağ, K., D. J. Dubowitz, E. J. Yoder, K. Restom, T. T. Liu, and R. B. Buxton, "Coupling of cerebral blood flow and oxygen consumption during physiological activation and deactivation measured with fMRI," *Neuroimage*, Vol. 23, pp. 148–155, Sep 2004.

139. Chen, J. J., and G. B. Pike, "Origins of the BOLD post-stimulus undershoot," *Neuroimage*, Vol. 46, pp. 559–568, Jul 2009.

140. Burke, M., and C. h. Bührle, "BOLD response during uncoupling of neuronal activity and CBF," *Neuroimage*, Vol. 32, pp. 1–8, Aug 2006.

141. Frahm, J., G. Krüger, K. D. Merboldt, and A. Kleinschmidt, "Dynamic uncoupling and recoupling of perfusion and oxidative metabolism during focal brain activation in man," *Magn Reson Med*, Vol. 35, pp. 143–148, Feb 1996.

142. Schroeter, M. L., T. Kupka, T. Mildner, K. Uludağ, and D. Y. von Cramon, "Investigating the post-stimulus undershoot of the BOLD signal–a simultaneous fMRI and fNIRS study," *Neuroimage*, Vol. 30, pp. 349–358, Apr 2006.

143. Segal, S. S., D. G. Welsh, and D. T. Kurjiaka, "Spread of vasodilatation and vasoconstriction along feed arteries and arterioles of hamster skeletal muscle," *J. Physiol. (Lond.)*, Vol. 516 (Pt 1), pp. 283–291, Apr 1999.

144. Ngai, A. C., K. R. Ko, S. Morii, and H. R. Winn, "Effect of sciatic nerve stimulation on pial arterioles in rats," *Am. J. Physiol.*, Vol. 254, pp. H133–139, Jan 1988.

145. Thijssen, D. H., E. A. Dawson, M. A. Black, M. T. Hopman, N. T. Cable, and D. J. Green, "Heterogeneity in conduit artery function in humans: impact of arterial size," *Am. J. Physiol. Heart Circ. Physiol.*, Vol. 295, pp. H1927–1934, Nov 2008.

146. Royl, G., C. Leithner, M. Kohl, U. Lindauer, U. Dirnagl, K. Kwong, and J. Mandeville, "The BOLD post-stimulus undershoot: fMRI versus imaging spectroscopy.," *Proc Intl Soc Mag Reson Med*, Vol. 9, 2001.

147. Hillman, E. M., A. Devor, M. B. Bouchard, A. K. Dunn, G. W. Krauss, J. Skoch, B. J. Bacskai, A. M. Dale, and D. A. Boas, "Depth-resolved optical imaging and microscopy of vascular compartment dynamics during somatosensory stimulation," *Neuroimage*, Vol. 35, pp. 89–104, Mar 2007.

148. Piechnik, S. K., P. A. Chiarelli, and P. Jezzard, "Modelling vascular reactivity to investigate the basis of the relationship between cerebral blood volume and flow under CO2 manipulation," *Neuroimage*, Vol. 39, pp. 107–118, Jan 2008.

149. Yoshino, H., T. Sakurai, X. S. Oizumi, T. Akisaki, X. Wang, K. Yokono, T. Kondoh, E. Kohmura, and K. Umentani, "Dilation of perforating arteries in rat brain in response to systemic hypotension is more sensitive and pronounced than that of pial arterioles: simultaneous visualization of perforating and cortical vessels by in-vivo microangiography," *Microvasc. Res.*, Vol. 77, pp. 230–233, Mar 2009.

150. Krüger, G., A. Kastrup, A. Takahashi, and G. H. Glover, "Simultaneous monitoring of dynamic changes in cerebral blood flow and oxygenation during sustained activation of the human visual cortex," *Neuroreport*, Vol. 10, pp. 2939–2943, Sep 1999.